



Seismic performance and vulnerability of gravity quay wall in sites susceptible to liquefaction

Stella Karafagka¹ · Stavroula Fotopoulou¹ · Anna Karatzetou¹ · Georgia Kroupi¹ · Kyriazis Pitilakis¹

Received: 10 January 2022 / Accepted: 24 October 2022 / Published online: 23 November 2022
© The Author(s), under exclusive licence to Springer-Verlag GmbH Germany, part of Springer Nature 2022

Abstract

Recent strong seismic events have highlighted the high vulnerability of port facilities resulting in significant physical damages and important socio-economic losses. The most widespread source of seismic damage to port structures is often not related to the ground shaking itself but to the induced phenomena principally associated to the liquefaction of loose, saturated soils that often prevails at coastal areas. In this context, this study aims at the investigation of the influence of soil liquefaction on the seismic performance and vulnerability of typical port gravity quay walls. Different gravity quay wall configurations are examined with varying base width/height ratios. Two-dimensional incremental dynamic analysis is conducted for the soil-quay wall system, under effective stresses using OpenSees software, considering a representative set of fifteen real ground motion records as input ground motion at the bedrock. Two numerical approaches are applied to investigate the effect of liquefaction on its seismic performance and vulnerability assessment: the first one without considering liquefaction, while the second considers the effects of liquefaction. The damage measure is defined in terms of the normalized seaward displacement. Fragility and vulnerability curves are finally derived in terms of different intensity measures and compared with available literature curves. Results show the important role of liquefaction in increasing the seismic vulnerability of the typical port quay wall.

Keywords Effective stress analysis · Fragility curves · Liquefaction · Numerical modelling · OpenSees · Port quay wall

1 Introduction

Ports constitute a key element in the transportation system globally, as they represent a major factor in the development of an area, sometimes located in areas susceptible to liquefaction. As quay walls accommodate importing and exporting activities, they are of the most essential assets of a port that might be strongly influenced by liquefaction hazard. Quay walls are earth retaining waterfront gravity structures, parallel to the shoreline, which create sufficiently deep vertical front to allow the approach, mooring, berthing, operations and maintenance of vessels and ships. The simplest type of gravity quay wall is block-type quay wall, that comprises concrete blocks constructed on a layer of crushed stone or gravel [33]. Experience gained from the

recent devastating seismic events, e.g. 1995 Kobe in Japan, 1999 Kocaeli in Turkey, 2011 Christchurch in New Zealand [13, 15, 33], among several others, highlighted the high susceptibility of port waterfront gravity structures to ground shaking and ground failure, including liquefaction and lateral displacement, that may result in extensive damages and high economic losses. Thus, the investigation of the seismic performance and vulnerability of waterfront gravity quay walls has become a concern to the waterborne transportation industry as well as the scientific community. Fragility curves are widely considered an efficient tool for estimating the seismic vulnerability of a structure, as they express the conditional probability of exceeding a certain damage limit state for a given ground motion intensity. It is also a useful tool in current performance-based earthquake engineering to link damage to the economic losses of structures.

Regarding the whole liquefaction process, including the onset of liquefaction, the process of generation, diffusion, and release of excess pore water pressure, and even the

✉ Stella Karafagka
stellak@civil.auth.gr

¹ Department of Civil Engineering, Aristotle University of Thessaloniki, PO BOX 424, 54124 Thessaloniki, Greece

development of liquefaction-induced displacements, it can be simulated with various numerical codes of fully coupled dynamic consolidation involving comprehensive constitutive models. The accuracy of numerical simulation depends on the soil material model and the accuracy of the parameters used in each model. Soil material constitutive models range from relatively simple cyclic stress–strain relationships to advanced ones incorporating yield surfaces, flow rules and hardening laws and can be formulated to describe soil behaviour with respect to total or effective stresses. Effective stress analysis allows the simulation of the generation, redistribution, and eventual dissipation of excess pore pressure during and after seismic shaking. Over the years, a plethora of numerical simulation platforms, e.g. OpenSees [44], FLAC [25], PLAXIS [8], etc., have been developed for advanced geotechnical engineering simulations involving liquefaction, most of which treat the saturated soil as two-phase media in which the differential equations governing the motion of soil and pore water flow are formulated by using Biot's theory [6] or mixture theory [7]. Moreover, some exciting progress has been achieved in the realm of constitutive modelling of the cyclic loading of non-cohesive soils, with emphasis on cyclic mobility and flow liquefaction, that may be divided into different categories depending on their fundamental characteristics, such as multi-surface plasticity models [62, 64], two-surface plasticity models [41, 42, 48], bounding surface plasticity models [5, 16] and generalized plasticity models [37, 50]. Each constitutive model has certain advantages and limitations. Most of the models are based on critical-state soil mechanics, which is an appropriate framework to use for this type of problem, as central to the current understanding is the existence of a critical-state line in the stress space and the existence of a flow liquefaction line [63]. In addition, some of these models consider the effects of fines, both plastic and non-plastic [18–20, 56], initial shear stress [63], viscosity [45], sample size [3], variation of permeability [41], etc.

Since the Great Hanshin Earthquake-damaged Kobe Port in 1995, significant advances have been made in the seismic behaviour and vulnerability of waterfront quay walls considering soil–structure interaction (SSI) and soil nonlinear behaviour in response to an earthquake, while performance-based design has been introduced for port structures [2, 10, 29, 30, 36, 52, 57]. More specifically, Pitilakis and Moutsakis [52] analyse the seismic behaviour of a gravity retaining quay wall and compared it with field observations. Kakderi and Pitilakis [29] propose seismic fragility curves for typical monolithic gravity quay walls, neglecting possible damages due to liquefaction effects. In the framework of UPGRADE research project [57], seismic fragility curves are proposed for typical block-type gravity quay walls, considering possible friction and

displacements between the interfaces of the construction blocks, again neglecting liquefaction-induced damages. Calabrese and Lai [10] present a seismic sensitivity analysis of a blockwork wharf, wherein the effects of inherent variations of ground motions and geotechnical quantities are investigated. Alielahi and Moghadam [2] investigate the influence of quay wall hunch on the seismic fragility, also ignoring soil liquefaction. Kamalzadeh and Pender [30] investigate the static and dynamic response of a gravity retaining wall for different Ricker wavelet excitations. Lee et al. [36] assess representative simplified dynamic analysis methods for the performance-based design of port gravity-type quay walls.

More recently, extensive research on the impacts that earthquake-induced liquefaction disaster events may have on the resilience of built assets and communities [27] has been conducted within a European research project titled LIQUEFACT (“Assessment and mitigation of liquefaction potential across Europe: a holistic approach to protect structures / infrastructures for improved resilience to earthquake-induced liquefaction disasters”). In the framework of this project, more emphasis was given in addressing the problem of microzoning a territory for earthquake-induced liquefaction hazard [35] or the effectiveness of several mitigation measures against liquefaction [14, 17] rather than estimating the fragility of structures or critical infrastructure. Thus, challenges remain for the seismic response and vulnerability assessment of quay walls considering liquefaction effects. Among the few vulnerability studies of waterfront gravity structures considering liquefaction, Ichii [21, 22] and Miraei and Jafarian [46] proposed analytical seismic fragility curves for gravity-type quay walls, while Calabrese and Lai [9] developed fragility functions for blockwork wharves using artificial neural networks, considering different geometries, type of failure mechanism and the effect of liquefaction occurrence. In most of these studies, the issue of different intensity measures (IMs) has attracted only limited attention.

In this context, the herein work aims to provide insight into the seismic performance of such widely spread class of structures as well as their vulnerability in terms of different IMs when soil conditions are susceptible to liquefaction. Different gravity quay wall configurations are examined with varying base width/height ratios of the coupled soil and the structure system, applying two-dimensional dynamic analyses under effective stresses using OpenSees [44]. Initially, we analyse for a number of strong ground excitations the response of three typical quay wall configurations when foundation soil conditions are prone to liquefaction. The results are presented and discussed in terms of acceleration time histories and peak values at different locations on the wall and the soil, as well as in terms of the

residual seaward displacements of the quay wall. Then, we compute the fragility and vulnerability curves of these wall configurations. The aim is to investigate the importance of taking into account the liquefaction susceptibility as well as the geometry of the quay wall on its seismic vulnerability assessment. To this respect, incremental dynamic analysis (IDA) [58] is conducted, and the fragility and vulnerability curves are derived for different IMs, namely peak ground acceleration on outcropping conditions (PGA_{rock}) or at surface (PGA_{surf}) or in terms of peak ground velocity at bedrock (PGV_{rock}), considering the normalized seaward displacement as the damage measure (DM). In general, it is shown that the vulnerability of the quay wall is generally decreased for stiffer quay wall configuration.

2 Numerical modelling

To study the important role of liquefaction on the seismic response and vulnerability of typical port gravity quay walls, different numerical models have been developed for different quay wall configurations with varying width W to height H (W/H) ratios. The potential effect of the liquefaction in the global seismic response and vulnerability of the gravity quay wall is studied considering a coupled soil–structure system under effective stress conditions where soil liquefaction capability is also considered using OpenSees software. The same set of numerical analyses are repeated ignoring liquefaction. This is achieved by setting the parameters defining the pore pressure build-up of the liquefiable layers equal to zero.

2.1 Soil and structure typologies under investigation

Based on the available geotechnical information, laboratory data and N_{SPT} values [4, 51], we consider two realistic soil profiles representative of the port area of Thessaloniki, Greece (Fig. 1). They are indicated as SP1 and SP2, with fundamental periods (T_0) equal to 0.71 s and 0.66 s, and shear wave velocity ($V_{s,30}$) equal to 234 and 240 m/s, respectively. The geotechnical characterization following the Unified Soil Classification System (USCS), the shear wave velocity (V_s) profiles and average N_{SPT} values for the two soil profiles are depicted in Fig. 1. These soil profiles refer to ground-type S following EC8 classification scheme [11], owing to the relatively high liquefaction potential of the subsoil layers that we quantitatively estimated according to the guidelines of Eurocode 8 (EC8)-Part 5 [12].

Regarding the structure, a typical gravity wall section of the Port of Thessaloniki has been selected (Fig. 2). The height of the quay wall is equal to 14.0 m and its base

width equal to 8.0 m ($W/H = 0.57$). Based on this initial section, two other more generic different configurations are chosen to study their vulnerability, both having the same height (10.0 m) but different base widths (6.0 and 8.0 m) corresponding to W/H ratios of 0.6 and 0.8, respectively. Figure 3 shows the geometry of these two other considered quay wall configurations and the surrounding backfill and mound gravel. The soil layers, the quay walls and their surrounding gravel characteristics are analytically described in the following.

2.2 Numerical models

The soil–structure system is modelled using OpenSees [44]. The soil mesh grid (50.0 m \times 150.0 m) has a total length three times its depth to avoid wave reflections at the vertical boundaries. Sufficiently dense discretization is achieved by using quadrilateral elements of 0.5 m \times 2.0 m (height \times length) considering that the lowest V_s equals 115.0 m/s. At the same time, the maximum frequency of interest is set to 10.0 Hz. Figures 4 and 5 illustrate the numerical models adopted for the three cases of gravity walls. The locations noted as A, B, C, D, and FF (point at the free-field surface), as well as the top of the quay wall (W_T), are used to capture the soil and quay wall seismic response.

The soil profiles are composed of different layers of cohesive and cohesionless soil materials (Fig. 1). Soil model SP1 is divided into eight soil layers while the soil model SP2 into six soil successive layers (Figs. 4 and 5). Saturated unit weights are used for the soil below the ground water level located at a depth of 2.0 m for both soil profiles, while nine-node quadrilateral elements are used for the foundation soil, the back-filled and mound gravel. These elements can simulate the dynamic behaviour of fully coupled (solid–fluid) material, following Biot’s theory of porous medium [6], as they have corner nodes with both displacement (u) and pore pressure (p) degrees of freedom (DOF) and interior nodes with only two displacement DOF.

The two-phase (solid–fluid) fully coupled (displacement–pore pressure, u-p) approach is applied, where the displacement of the soil and the pore pressure are computed simultaneously and interactively at each time step, which can simulate permanent accumulation of shear strain in cohesionless soils during soil liquefaction. The constitutive model employed to describe the soil behaviour in OpenSees depends on the multi-yield-surface plasticity concept [53], with some modifications by Yang [60], namely two distinct phases of soil response were added: (i) a perfectly-plastic slip strain phase (without contraction or dilation) represented by a robust strain-space formulation, followed by (ii) a strongly dilative/contractive phase

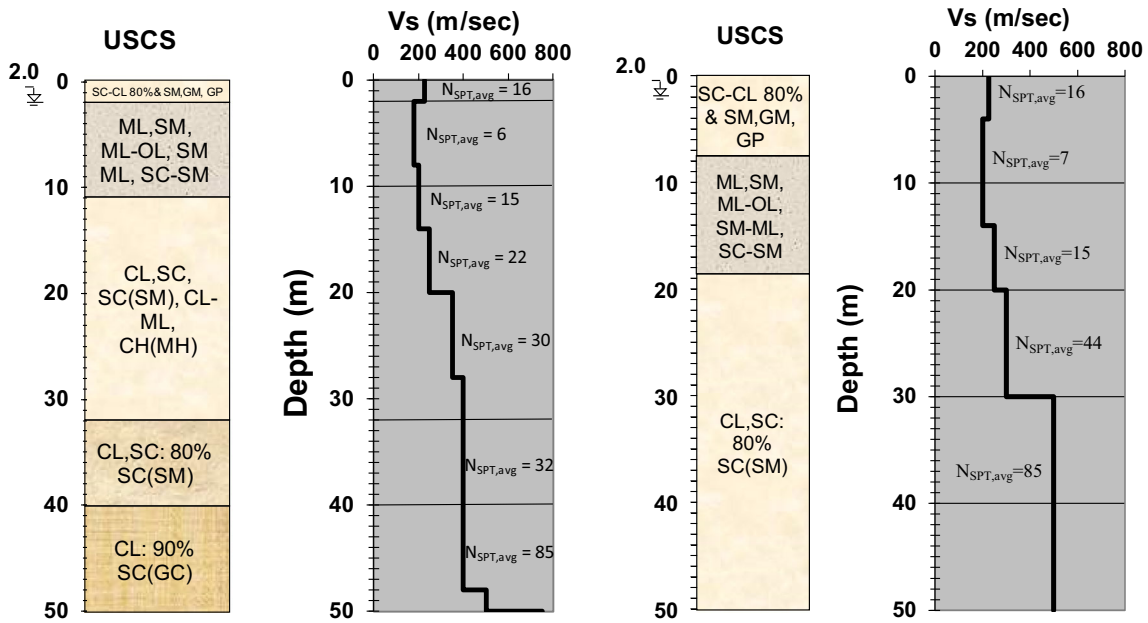


Fig. 1 Geotechnical profiles SP1 (left) and SP2 (right) following the USCS classification scheme, V_s profile and average N_{SPT} values

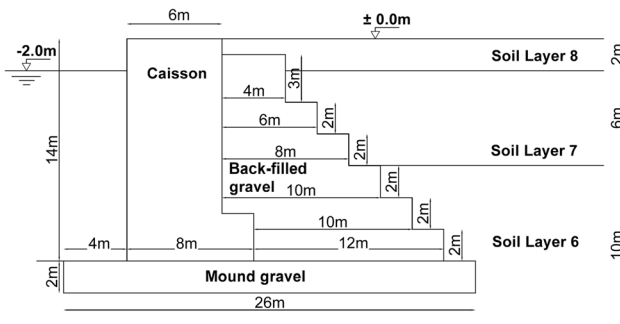


Fig. 2 Geometry of the Thessaloniki port quay wall with $W/H = 0.57$ and its surrounding backfill and mound gravel

beneath the failure envelope. The major components of the plasticity model are the yield surface, the flow rule, and the hardening law. During the gravity load application, a linear elastic material behaviour is used, while during the subsequent dynamic loading the soil elements constitutive

behaviour is switched to elastoplastic. A purely deviatoric kinematic hardening rule [53] is employed to simulate the hysteretic behaviour of soil under cyclic loading, thus all yield surfaces correspond to stress space within the failure envelope [49, 60] and comply with Masing loading–unloading–reloading criteria [43]. Under drained monotonic shear loading, the nonlinear stress–strain backbone curve in this model (after Prevost [53] and Parra [49]) is represented by piecewise linear segments with a certain number of similar yield surfaces or user-defined pairs of normalized secant shear modulus versus shear strain points. The cohesionless soil layers are modelled using the “PressureDependMultiYield02” (PDMY02) elastic–plastic material of OpenSees [44]. The yield surface is a function of friction angle and cohesion, the yield function follows the shape of the Drucker–Prager criterion (conical Drucker–Prager yield surfaces, after Prevost [53], Yang [60] and Parra [49]), while plasticity is expressed through a

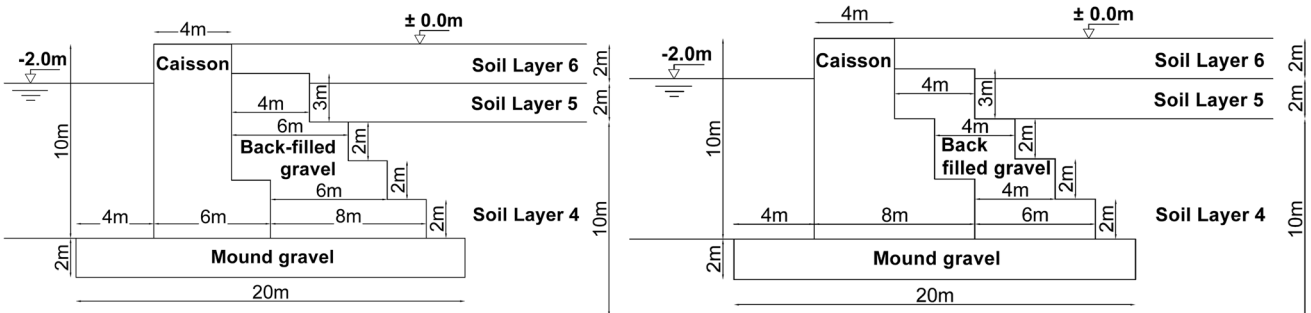


Fig. 3 Geometry of the two generic gravity quay wall configurations with W/H ratios equal to 0.6 (left) and 0.8 (right) and the surrounding backfill and mound gravel

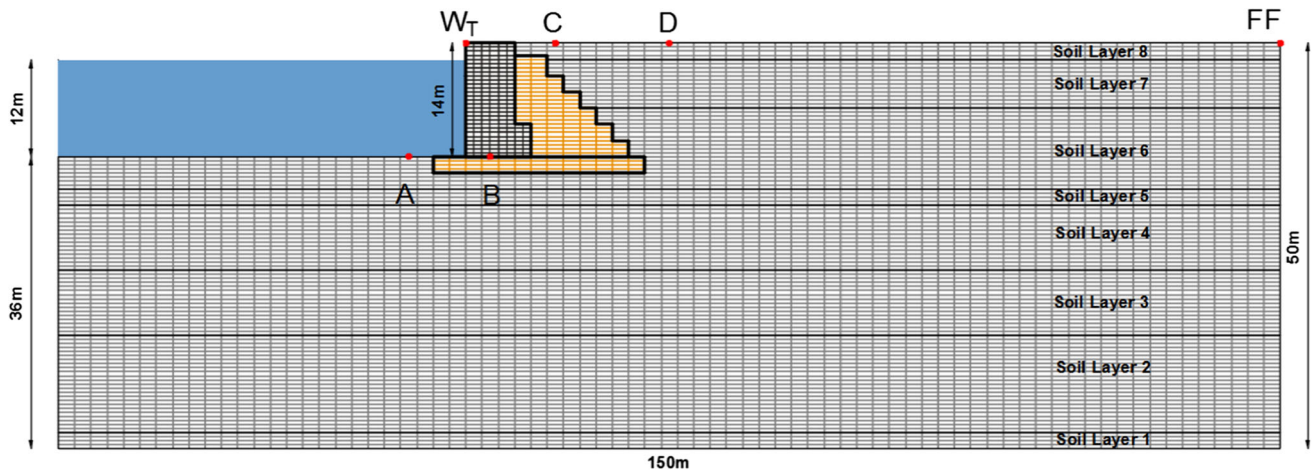


Fig. 4 Geometry of the finite element soil–structure model for the Thessaloniki port typical gravity quay wall with the soil profile SP1 along with the locations of the nodes used to capture the soil and quay wall seismic response

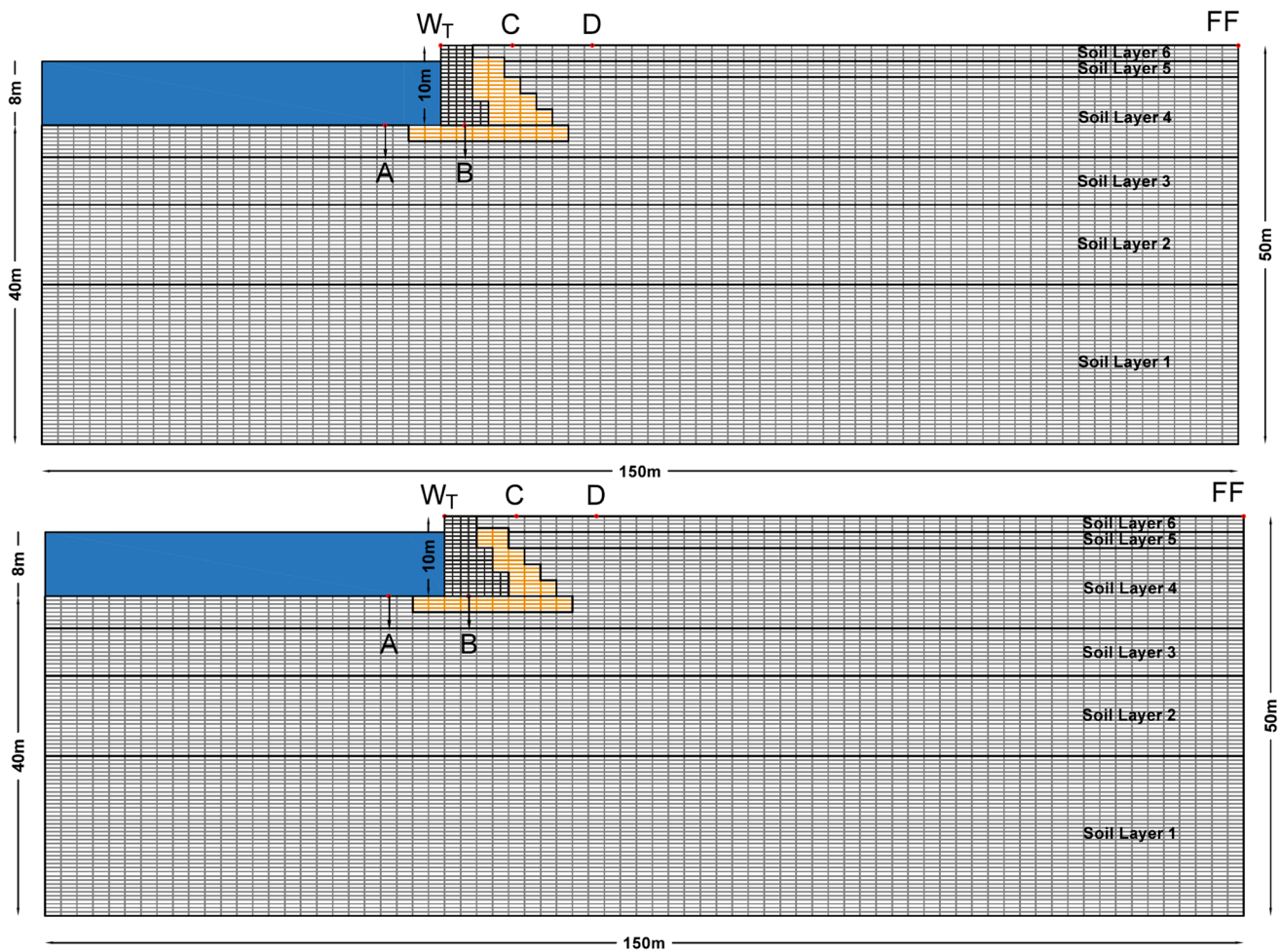


Fig. 5 Geometry of the finite element soil–structure models for the two generic quay wall configurations with W/H ratios equal to 0.6 (top) and 0.8 (bottom) with the soil profile SP2 along with the locations of the nodes used to capture the soil and quay wall seismic response

Table 1 SP1 soil properties used in OpenSees

Layer Thickness (m)	Soil layer	Model	ρ (Mg/m ³)	V_s (MPa)	G_r (MPa)	B_r (MPa)	ϕ (o)	c (kPa)
2m	8 (surface)	PDMY02	1.835	225	92.9	279.0	39	-
6m	7	PDMY02	1.886	180	61.1	183.0	32	-
10m	6	PDMY02	2.039	200	81.6	245.0	33.5	-
2m	5	PIMY	2.039	250	127.0	382.0	25	23
8m	4	PIMY	2.039	350	250.0	749.0	25	23
8m	3	PIMY	2.141	400	343.0	1030.0	25	25
12m	2	PIMY	2.141	400	343.0	1030.0	25	40
2m	1	PIMY	2.141	500	535.0	1610.0	20	50

* Cohesionless (PDMY02) and cohesive (PIMY) soil models

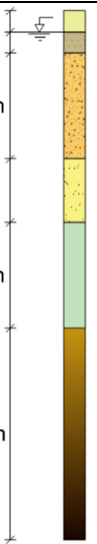
non-associative plastic flow rule [49]. This flow rule can handle the contractive/dilative soil behaviour stimulated by shear loading to efficiently depict the interaction between shear and volumetric responses. The cohesive soil layers are modelled with the “*PressureIndependentMultiYield*” (PIMY) material. This describes an elastic–plastic material in which the volumetric stress–strain response is linear elastic and independent of the deviatoric response, which simulates the monotonic or cyclic response of materials whose shear behaviour is insensitive to changes of the confinement pressure. The yield surface is solely a function of the undrained shear strength, the yield function is assumed to follow the Von Mises criterion (cylindrical Von Mises yield surfaces, after Prevost [53], Yang [60] and Parra [49]), while plasticity, which exhibits only in the deviatoric stress–strain response, is defined via the multi-yield surface plasticity model with an associative plastic flow rule. This flow rule considers that the incremental plastic strain vector is normal to the yield surface. Further information on this advanced constitutive model and basic concepts of plasticity can be found in Stewart et al. [55]. It should be noted that although the soil profiles described above are liquefiable, in the second modelling approach liquefaction potential is not considered. This is achieved by setting the parameters defining the pore pressure build-up of the potentially liquefiable layers equal to zero [9, 31].

The PDMY02 plasticity-based soil constitutive model [64] used herein directly considers excess pore pressure redistribution and SSI in evaluating the liquefaction hazard and impacts on structures and has been calibrated by several researchers and is widely used for geotechnical earthquake engineering applications [34, 61]. Despite some inevitable limitations, which is also found in other existing literature models, namely the possible underestimation of the post-liquefaction volumetric strains [61], the difficulty of capturing the full dilation amplitude after liquefaction launch and the potential overestimation of the soil damping at large strains [54], it is considered as appropriate and accurate enough for the analyses performed in this work.

For each soil layer, the soil properties, namely the shear wave velocity (V_s), the mass density (ρ), the cohesion (c), the friction angle (ϕ) at the peak shear strength and Poisson’s ratio ν (considered equal to 0.35), are defined, while the reference low-strain shear (G_r) and bulk (B_r) moduli are also estimated. The mass density of the materials corresponds to the total mass densities, thus for the soil layers that overlay or underlay the groundwater table dry or saturated conditions should be reflected, respectively. Tables 1 and 2 summarize the soil properties adopted in OpenSees for each soil layer for soil profiles SP1 and SP2, respectively. For soils susceptible to liquefaction, a set of parameters that describe and control the mechanism of the

Table 2 SP2 soil properties used in OpenSees

Layer Thickness (m)	Soil layer	Model	ρ (Mg/m ³)	V_s (MPa)	G_r (MPa)	B_r (MPa)	ϕ (o)	c (kPa)
2m	6 (surface)	PDMY02	1.835	225	92.9	279.0	39	-
2m	5	PDMY02	2.039	225	103.0	310.0	35	-
10m	4	PDMY02	1.886	200	75.4	226.0	32	-
6m	3	PDMY02	2.141	250	134.0	401.0	33.5	-
10m	2	PIMY	2.141	300	193.0	578.0	25	25
20m	1	PIMY	2.141	500	535.0	1610.0	25	40



*Cohesionless (PDMY02) and cohesive (PIMY) soil models

accumulation of completely plastic shear deformation caused by liquefaction are also defined according to the proposed values of Yang et al. [64]. Regarding the gravel backfill, it is simulated employing the “PressureDependMultiYield02” material, where the mass density is set equal to 1.8 Mg/m³ above the water table and 2.1 Mg/m³ below the water table, while the friction angle ϕ , G_r and B_r are defined equal to 40°, 189 and 567 MPa, respectively.

All three quay wall configurations are modelled using standard four-node plane strain quad elements 0.5 m × 1.0 m, with nodes that have only two translational DOF. Sliding between blocks is not allowed. The quay wall is modelled as an “ElasticIsotropic” material, considering Young’s Modulus (E) equal to $E = 27000$ MPa, mass density equal to $\rho = 2.4$ Mg/m³ and a Poisson’s ratio equal to $\nu = 0.2$. There is no interface between the quay wall and the surrounding soil material resulting in equal displacements between the quay wall and the backfill.

The hydraulic boundaries of the model are also assigned. As the ground water table is located at -2.0 m for both soil profiles, all the pore pressure nodes that lie above this level have their pore pressure degrees of freedom fixed. This creates a water drainage path which allows the water to escape to the adjacent elements and ensures that pore pressure is maintained to zero, as no pore pressure

is built up in the area above the groundwater table. The same constrain is assigned to the nodes of the seabed which lie at the foot of the quay wall, as they are submerged beneath the water and to the backfill nodes which are in contact with the quay wall as well. The body of water and the dynamic effects it causes are incorporated into the model in a way that does not affect the effective stresses of the soil elements. The water forces are applied to the nodes of the seabed as vertical nodal masses. The water mass value for each of these nodes is derived by multiplying the depth of the water, the water’s mass density, the half of the distance to adjacent nodes and the thickness of the elements this mass refers to. A similar procedure is followed to assign the water forces applied at the vertical front face of the quay wall. In this case, horizontal masses are defined, calculated by applying a triangular distribution of the hydrostatic forces considering that the maximum depth is 12.0 and 8.0 m for SP1 and SP2, respectively.

Special boundary conditions are also defined to avoid the presence of wave reflections and ensure that free-field conditions exist at the lateral boundaries of the soil model. More specifically, the elements in the edge lateral columns of the mesh are given a significantly increased-practically infinite-thickness, so they appear to be adequately more massive than the rest of the elements in the interior of the mesh. In addition, we achieve periodic boundary

Table 3 Catalogue of seismic records (<http://www.isesd.hi.is/>) applied for the IDA

Waveform ID	Earthquake name	Date	M_w	R (km)	$PGA_{initial}$ (m/s ²)	$PGA_{corrected}$ (m/s ²)	Fault mechanism	EC8 site class
000134	Friuli (aftershock)	15/9/1976	6.0	14	2.586	2.649	Thrust	B
000149	Friuli (aftershock)	15/9/1976	6.0	12	1.339	1.373	Thrust	A
000229	Montenegro (aftershock)	24/5/1979	6.2	17	1.708	1.766	Thrust	B
000242	Valnerina	19/9/1979	5.8	5	2.012	2.060	Normal	A
000242	Valnerina	19/9/1979	5.8	5	1.510	1.472	Normal	A
000414	Kalamata	13/9/1986	5.9	11	2.670	2.747	Normal	B
000594	Umbria Marche 2	26/9/1997	6.0	11	5.138	5.592	Normal	B
000651	Umbria Marche (aftershock)	6/10/1997	5.5	5	1.838	2.060	Normal	A
000763	Umbria Marche	26/9/1997	5.7	23	1.645	1.668	Normal	A
000990	Lazio Abruzzo (aftershock)	11/5/1984	5.5	15	1.411	1.373	Normal	A
001714	Ano Liosia	7/9/1999	6.0	14	2.159	2.256	Normal	B
001932	Patras	14/7/1993	5.6	9	3.337	3.434	Strike-slip	B
003802	SE of Tirana	9/1/1988	5.9	7	4.037	3.826	Thrust	A
006040	Kefallinia island	23/1/1992	5.6	14	2.223	2.060	Thrust	B
006115	Kozani	13/5/1995	6.5	17	2.039	2.158	Normal	A

conditions by bounding together the translational DOF for the nodes on either side of these lateral columns, so they perform equal displacements both in the horizontal and in the vertical direction.

Finally, the finite rigidity of the underlying bedrock is idealized, considering an elastic half-space. For this reason, a Lysmer and Kuhlemeyer [40] viscous damper is applied in the horizontal direction to the soil model base to account for the finite rigidity of the underlying half-space, setting a bedrock shear wave velocity equal to 750.0 m/s and mass density equal to 2.2 Mg/m³. To set the Lysmer–Kuhlemeyer dashpot constitutive behaviour in the horizontal direction, we use the viscous uniaxial material. This material model requires a single input defined according to Joyner and Chen [28] by multiplying the mass density and the shear wave velocity of the underlying bedrock, including the soil profile base area, namely the dashpot coefficient (c). This is scaled by the area of the soil model base to ensure that equivalent loading is imposed. Moreover, for the elastic half-space modelling, the nodes at the

soil model base are all assigned equal horizontal displacements and are fixed in the vertical direction. To consider energy dissipation during seismic excitation, mass and stiffness proportional Rayleigh damping is assigned, the level controlled by the damping ratio (for the soil material equal to 2.0%).

3 Seismic ground motions

The seismic excitation applied along the base of the models comprises a suite of fifteen real acceleration time histories from different earthquakes (Table 3) chosen from the European Strong-Motion Database (www.isesd.hi.is). These seismic ground motions correspond to stiff or rock-type soils (soil types A and B as stated in EC8). We selected them in so their moment magnitude (M_w) and epicentral distance (R) range between $5.5 < M_w < 6.5$ and $0.0 < R < 45.0$ km, respectively. They are covering a wide range of peak ground acceleration (PGA) from 0.13 g

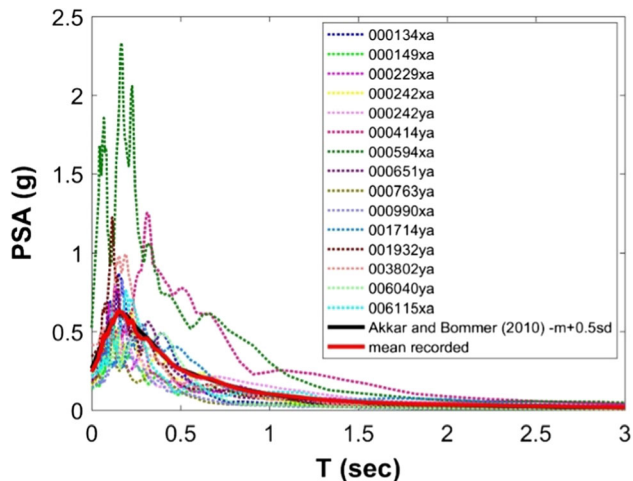


Fig. 6 Elastic response spectra of the selected earthquake records and their mean elastic response spectrum in comparison with the corresponding median plus 0.5 standard deviations Akkar and Bommer [1] response spectrum

to 0.51 g. We applied the following main criterion for their selection; the mean acceleration spectrum of the selected records to match the corresponding 5% damped median plus 0.5 standard deviations Akkar and Bommer [1] spectrum. We performed the optimization process with REXEL [23], a software that enables receiving combinations of accelerograms, that on average are accordant with the reference spectrum. The selected records cover various earthquake excitations in terms of amplitude, significant duration, and frequency content. The catalogue of the selected real seismic records is presented in Table 3. Figure 6 shows the 5% elastic response spectra of the selected earthquake records and their mean elastic response spectrum compared to the corresponding median plus 0.5

standard deviations of Akkar and Bommer [1] elastic response spectrum. The matching is satisfactory. These records are then filtered between 0.25 and 15 Hz, using a fourth-order bandpass Butterworth type filter. Baseline correction linear type is also applied. Table 3 also presents the values of $PGA_{corrected}$ obtained from the corrected accelerograms used for the analyses. Among the selected time histories it is worth to notice that the frequency content of the Kalamata and Umbria Marche 2 earthquake records (ID 414 and 594, respectively) is quite distinct compared to the other records (Fig. 6), as they are characterized by long-period pulses unlike the other high-frequency records.

4 Seismic response of the gravity quay wall

The effect of soil liquefaction on the seismic response of the typical gravity quay wall of the Port of Thessaloniki with W/H equal to 0.57 is illustrated below, conducting two sets of seismic analyses for the two conceptual modelling approaches using as input the earthquake records of Table 3. Layers of potential liquefaction are identified by the loss of effective confining stress (equal to zero) which is also verified by the corresponding stress–strain loops (e.g. at -15.0 m depth at free-field conditions as shown in Fig. 7). Indicatively, Fig. 7 presents the computed effective confinement profile and stress–strain hysteresis loops at specific depth for Kalamata earthquake motion (ID 414 record) for the two approaches, considering or neglecting soil liquefaction.

For the case that we consider liquefaction, the hysteresis loops corresponding to the time before the onset of liquefaction are smooth and are dominated by steeper slope,

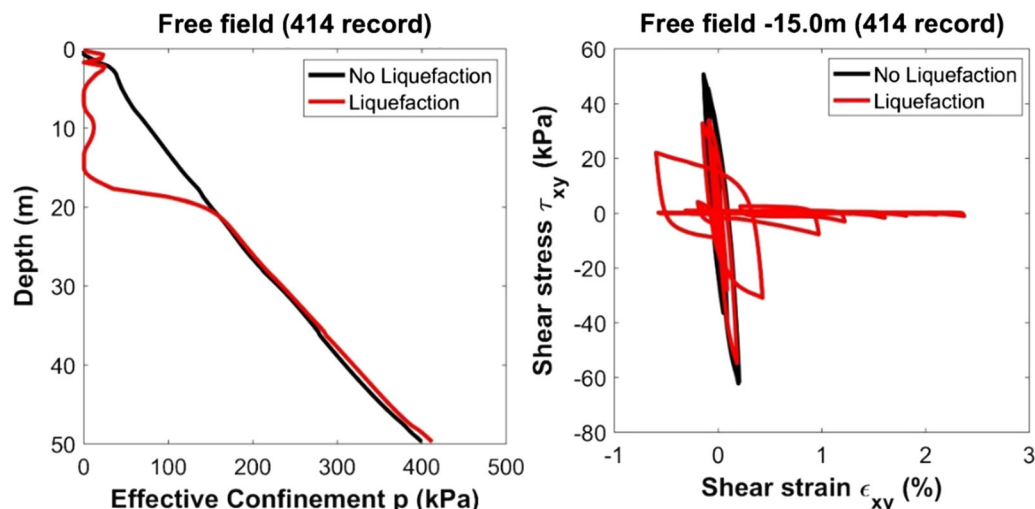


Fig. 7 Confinement stresses at free field conditions (left) and corresponding stress–strain hysteresis loops at -15.0 m depth (right) for the Kalamata (ID 414) record and for the quay wall with W/H = 0.57 and SP1 soil conditions

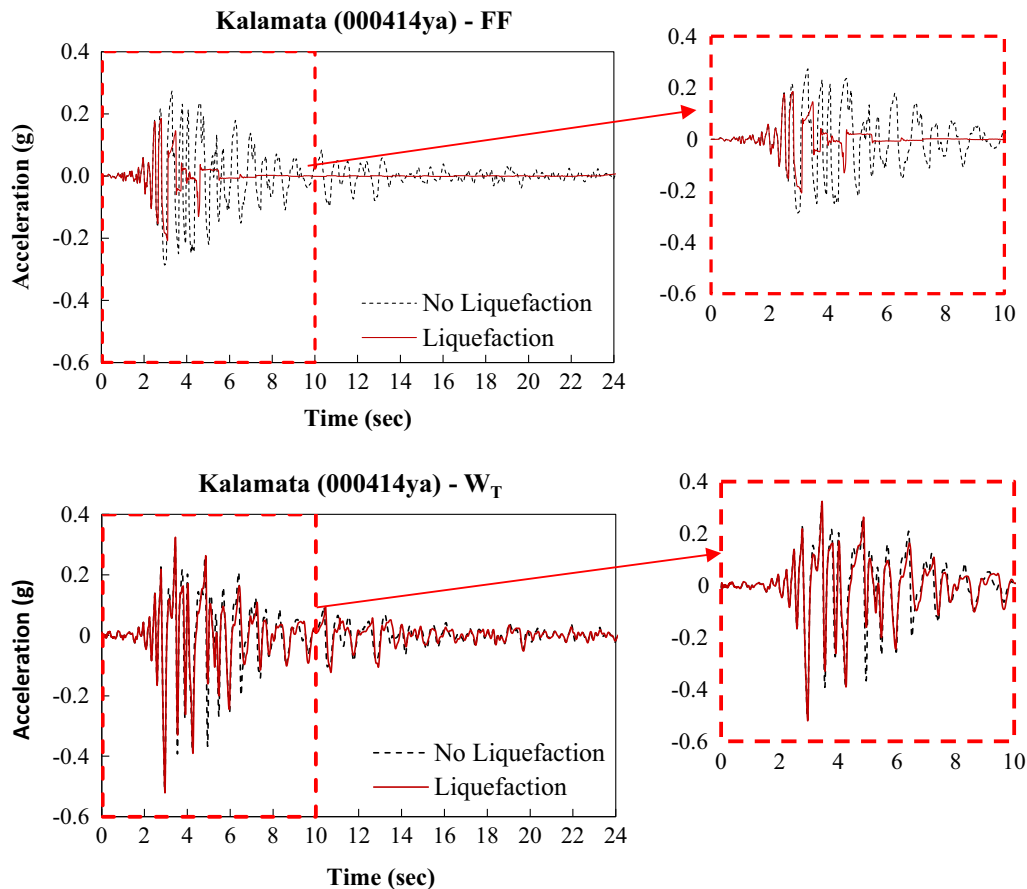


Fig. 8 Comparison of the acceleration time histories computed at free-field conditions FF (top) and on the wall W_T (bottom) for the quay wall with $W/H = 0.57$ and SP1 soil conditions for the Kalamata ID 414 record

indicating greater values of the dynamic shear modulus which represents the shear stiffness of the soil, while after a specific point, a change in the pattern of the stress–strain loops is observed. Specifically, the circles are characterized by large shear strain amplitudes and adequately small shear stresses, leading to a radical decrease in the shear stiffness and accumulation of large shear strains (Fig. 7).

The effect of liquefaction on the acceleration time histories and the frequency content of the motion at free-field soil surface and on the quay wall is also examined. Indicatively, the acceleration time histories for the two considered approaches at the free-field (FF) and on the wall (W_T) for the Kalamata record (ID 414) are presented in Fig. 8. Regarding the computed acceleration time history at the FF, as shown in Fig. 8 (top) for Kalamata (ID 414) record, liquefaction occurrence causes seismic energy dissipation and leads, as expected, to significant reduction in the strong ground motion duration. The amplitudes of the ground motion in the case where liquefaction occurs are decreased, compared to the corresponding values ignoring liquefaction.

Contrary to the free-field conditions, it is observed (Fig. 8, bottom) that the liquefaction didn't alter the computed acceleration time histories on the top of the wall compared to the no-liquefaction case. The reason of this phenomenon may be attributed to the oscillation of the rigid wall in a coupled system when receiving a rather similar seismic excitation at its base. Indicatively, computed acceleration time histories at different locations with the Kalamata (ID 414) record used as rock input motion, are presented for the two approaches in Fig. 9.

In Fig. 10, we summarize the computed PGA values for all input motions at the top of quay wall (W_T) and at the different other locations (i.e. FF, C and D) for the two cases, i.e. considering or not liquefaction for the quay wall configuration with W/H ratio equal to 0.57. The main observation from the analyses of the spatial evolution of the PGA values is that the peak acceleration values on the wall are amplified independently of the presence or not of liquefaction while they are progressively decreased moving away from the wall to the free-field values (Fig. 10 locations FF and D) due to the increase of the importance of liquefaction and nonlinear site effects. The closer we are to

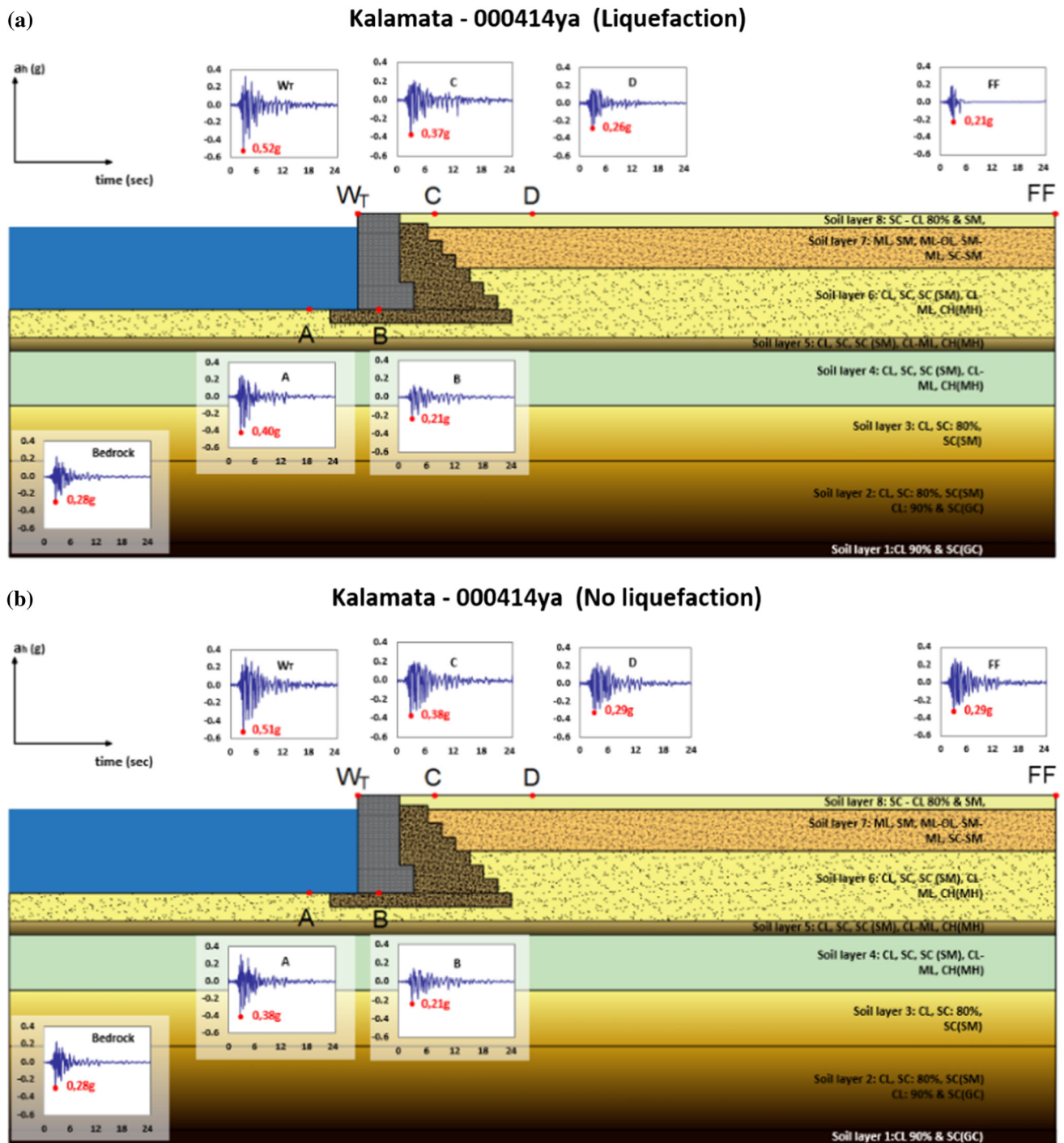


Fig. 9 Acceleration time history response at the various sites of the model for the quay wall with $W/H = 0.57$ and SP1 for Kalamata—ID 414 input motion **a** considering or **b** neglecting liquefaction

the wall the more the ground response is controlled by the oscillation of the wall itself. It should be also notified that the red points depict the results of the analysis for Umbria Marche 2 (ID 594) input motion where the analysis failed, and the results are presented only for completeness reasons. Moreover, for the liquefiable case at FF (Fig. 10, top-right) it is observed that for a PGA_{rock} value lower than

approximately 0.2 g there is still an amplification of the PGA relative to PGA_{rock} , while for PGA_{rock} values higher than 0.2 g the PGA value of the seismic motion attenuates due to liquefaction. These observations are in accordance with the results of the study of Lopez-Caballero and Modaresi Farahmand-Razavi [38].

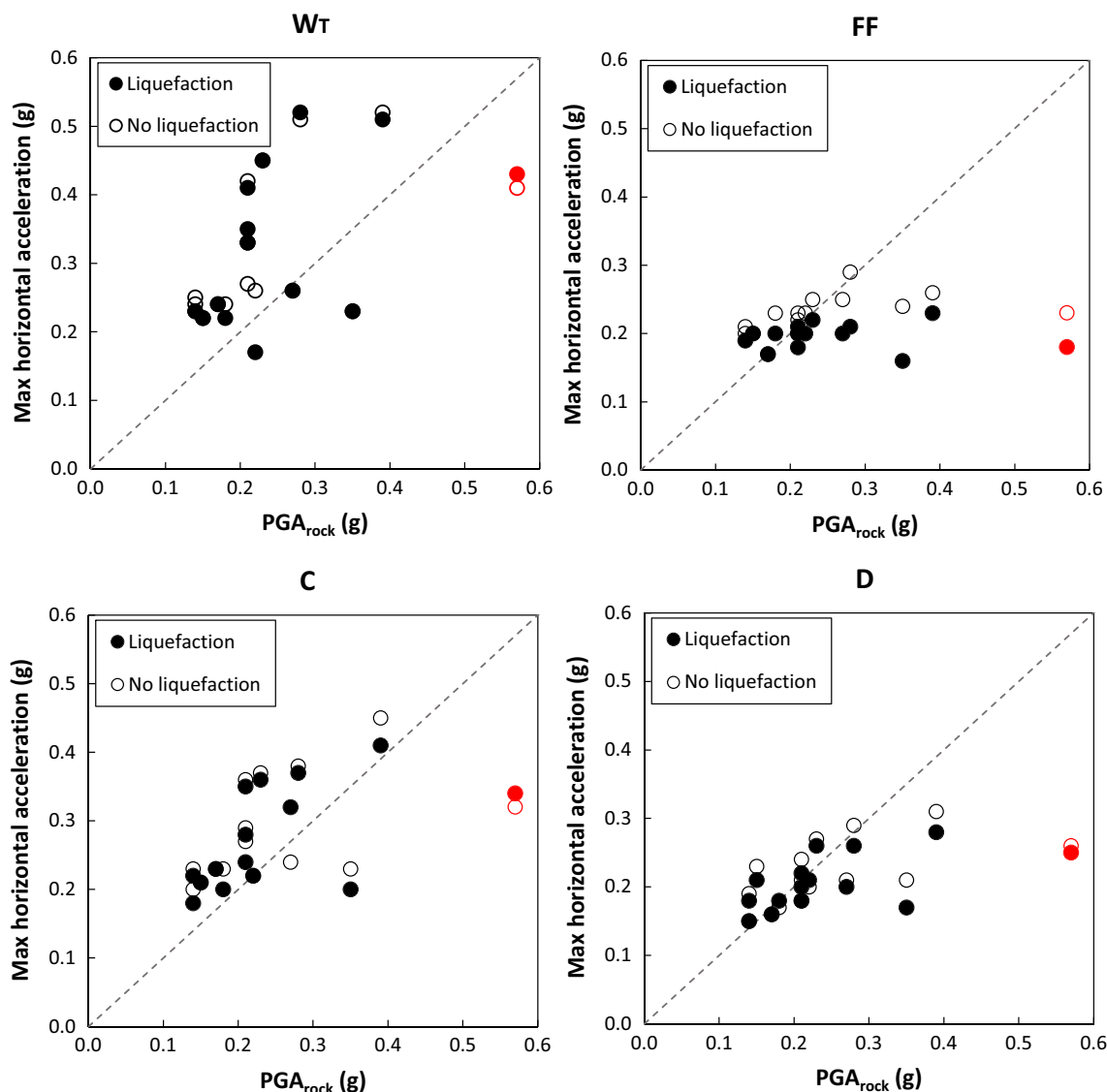


Fig. 10 Maximum horizontal acceleration—PGA_{rock} pairs at different locations: *W_T* (top-left), *FF* (top-right), *C* (bottom-left) and *D* (bottom-right) for the two cases allowing (solid circles) or not liquefaction for the quay wall configuration with *W/H* ratio equal to 0.57

The computed residual seaward displacements and the permanent vertical displacements at the top of the rigid wall variation with PGA_{rock} and PGV_{rock} for both approaches when considering or neglecting liquefaction for the quay wall configuration with *W/H* ratios equal to 0.57 are presented in Fig. 11. The red points again depict the results of the analyses failed, and the results are presented only for completeness reasons. It is clear that in the case of liquefaction the seaward permanent displacements of the wall are much higher, compared to the non-liquefaction case, which nevertheless are not negligible. For example, for the quay wall configuration with *W/H* ratio equal to 0.57 on SP1, for rock-basement excitations of 0.2–0.3 g the average value of the horizontal permanent displacement without liquefaction are on the order of 5.0 cm, and they are

doubled in case liquefaction is considered. This is noticeable either considering PGA_{rock} or PGV_{rock}. A similar trend is observed for the vertical displacements, where, however, the values are as expected lower compared to the horizontal displacements. More specifically, for the quay wall configuration with *W/H* ratio equal to 0.57 on SP1, the permanent horizontal displacements vary from 2.3 to 60.3 cm when we consider soil liquefaction and from 1.9 to 31.9 cm when liquefaction is neglected, while the permanent vertical displacement values range between 2.1 and 17.8 cm for the liquefiable case compared to those of the non-liquefiable case that vary between 1.9 and 11.6 cm.

To better understand the differences between the two approaches at the quay wall response in terms of displacements, we present in Fig. 12 the ratios of the residual

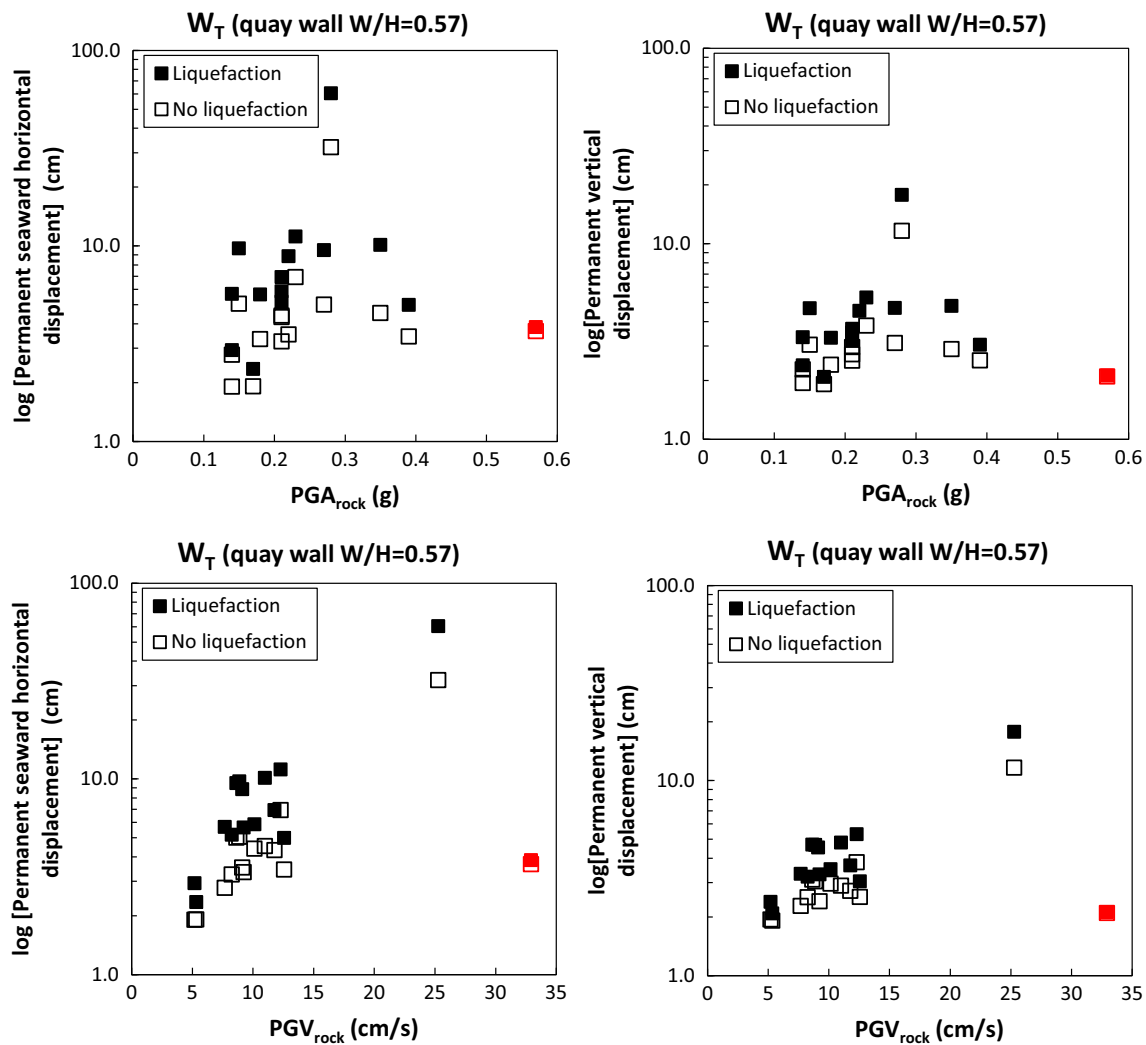


Fig. 11 Permanent horizontal displacement (left) and permanent vertical displacement (right) at the W_T variation with PGA_{rock} (top) and PGV_{rock} (bottom) with (solid rectangles) and without liquefaction for the quay wall configuration with W/H ratio equal to 0.57 and SP1

horizontal and vertical displacement values at the W_T variation with PGA_{rock} and PGV_{rock} for the liquefiable case to the corresponding ones for the non-liquefiable case for the two comparable quay wall configurations. Again the red points show the results of the analyses failed, and the results are presented only for completeness reasons. It is obvious that the seaward residual displacements as well as the vertical displacements of the wall are much higher (2 to 5 times) when considering liquefaction. This trend is more intense for the stiffer quay wall configurations when W/H ratio increases.

In addition to PGA_{rock} , we observe the trend that PGV_{rock} may better capture the effects of liquefaction on the residual displacements [31]. The selection of the IM that adequately correlates with the structural damage is a key issue in the fragility assessment, and the investigation of alternative IMs is facilitated via regression analysis with engineering demand parameters (EDP) results from the

nonlinear dynamic analysis of a structure [39]. In addition, there are several studies that deal with the efficiency and sufficiency of an IM for deriving vulnerability curves [26, 59]. In this case, PGV_{rock} provides an improved correlation between the wall permanent displacements and PGV_{rock} and seems to be better correlated with structural damage compared to PGA_{rock} , as was also found in Karafagka et al. [32] statistically. For this reason, it has been decided to develop fragility and vulnerability curves also in terms of PGV_{rock} .

5 Vulnerability assessment

The vulnerability analysis is conducted applying the IDA approach [58]. We used OpenSees [44] to develop seismic fragility curves in the presence of liquefaction effects for different damage limit states through statistical correlation

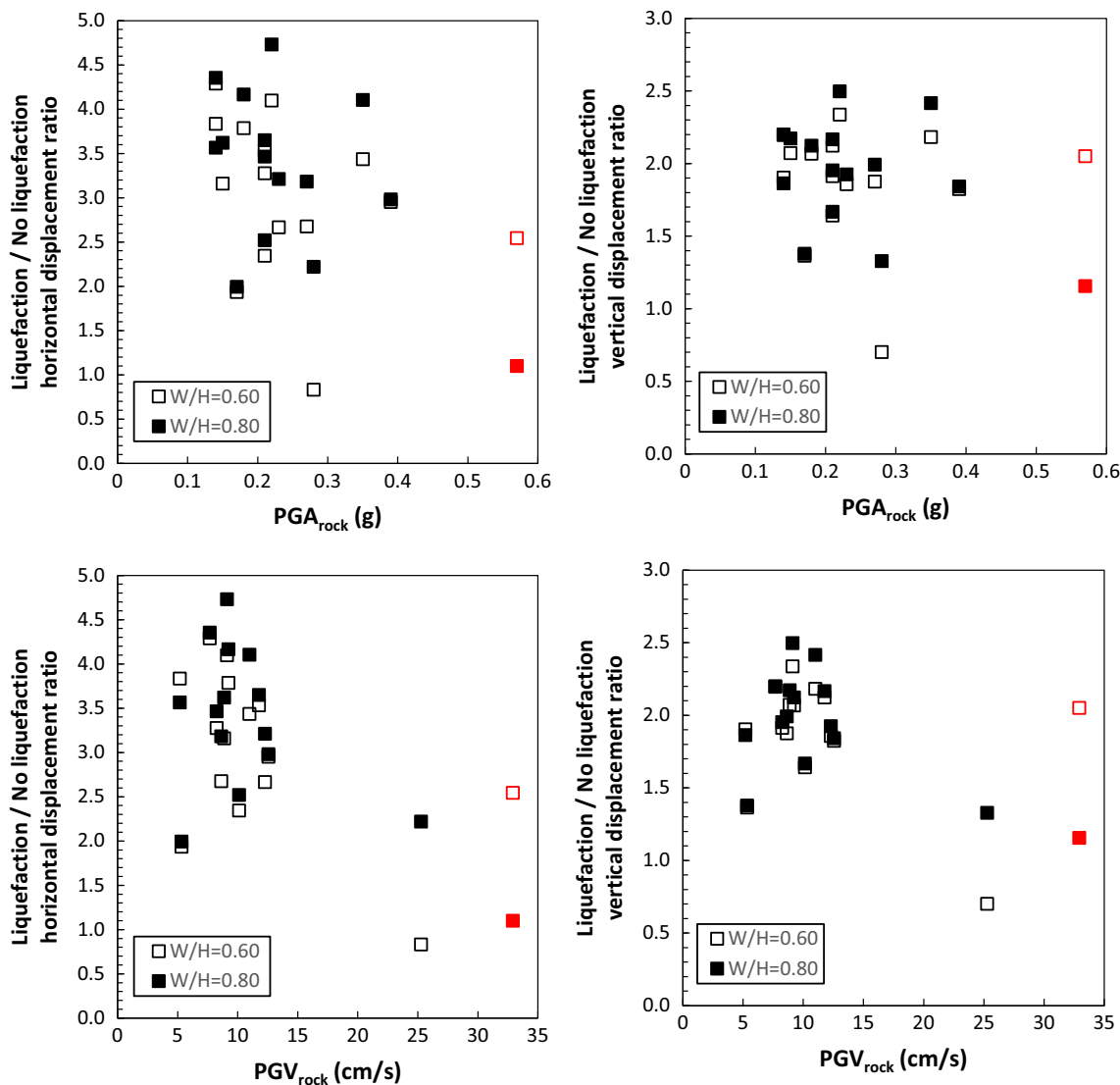


Fig. 12 Ratios of the permanent horizontal (left) and vertical displacement (right) values computed at the W_T variation with PGA_{rock} (top) and PGV_{rock} (bottom) for the liquefiable case to the corresponding ones for the non-liquefiable case for the two quay wall configurations with W/H ratios equal to 0.6 (top) and 0.8 (bottom) and SP2 soil conditions

of the calculated DM with appropriate IMs. The same analysis is conducted without liquefaction occurrence by setting the parameters defining the pore pressure build-up of the liquefiable layers equal to zero. The IMs are initially expressed in terms of the peak ground acceleration (PGA_{rock}) at outcropping conditions. This IM is considered more appropriate due to its simplicity and practicality. Hence, we run IDA for the considered finite element soil-structure models by applying the fifteen incrementally scaled records at bedrock, considering a first (elastic) run at 0.05 g, then an initial step of 0.1 g, increased by a constant step of 0.1 g, up to 0.6 g. We perform a sequence of seven runs on each record. Different engineering demand parameters (EDPs) have been considered to assess the seismic performance of the considered generic quay wall

configurations, namely (a) the normalized seaward horizontal displacement (horizontal displacements divided by the wall height), (b) the absolute horizontal displacement and (c) the absolute vertical displacement. The DM is finally expressed in terms of the normalized seaward displacement (horizontal displacements divided by the wall height), which is shown to result as the most appropriate Damage Metric from the viewpoint of quay wall performance [24].

5.1 Definition of limit states

The definition of realistic damage states is of paramount importance for the development of fragility curves. Four damage limit states are defined in terms of normalized

Table 4 Description of damage states for waterfront structures subject to ground failure according to NIBS [47]

Damage states	Description
Minor	Minor ground settlement resulting in few piles (for piers/seawalls) getting broken and damaged. Cracks are formed on the surface of the wharf. Repair may be needed
Moderate	Considerable ground settlement with several piles (for piers/seawalls) getting broken and damaged
Extensive	Failure of many piles, extensive sliding of piers, and significant ground settlement causing extensive cracking of pavements
Complete	Failure of most piles due to significant ground settlement. Extensive damage is widespread at the port facility

Table 5 Damage state values for waterfront structures according to PIANC [24]

Damage states	u_x/H_{wall} (%)
Minor	< 1.5
Moderate	1.5–5.0
Extensive	5.0–10.0
Complete	> 10.0

Table 6 Damage limit state values in terms of normalized residual seaward displacement (u_x/H_{wall}) adopted for the typical quay wall

Limit states	u_x/H_{wall} (%)
Minor	0.75
Moderate	3.25
Extensive	7.50
Complete	12.50

residual seaward displacement (u_x/H_{wall}), describing the exceedance of minor, moderate, extensive and complete damage of the quay wall. The qualitative description of each damage state for quay walls is provided in Table 4. In this study, the damage limit states are defined based on the existing literature (i.e. PIANC [24], Table 5), while the adopted (mean) limit state values are shown in Table 6.

5.2 Development of seismic fragility and vulnerability curves

Fragility curves describe the probability of exceeding a predefined level of damage under a seismic excitation of a given intensity. The results of the nonlinear numerical

analysis (PGA_{rock} and u_x/H_{wall} , PGV_{rock} and u_x/H_{wall} as well as PGA_{surf} and u_x/H_{wall} data pairs) are used to derive fragility curves expressed as two-parameter lognormal distribution functions. The following equation gives the cumulative probability of exceeding a damage limit state conditioned on a measure of the seismic motion intensity IM:

$$P[LS | IM] = \Phi \left(\frac{\ln(IM) - \ln(\widehat{IM})}{\beta} \right) \tag{1}$$

where Φ is the standard normal cumulative distribution function, LS is the damage limit state, IM is the intensity measure of the earthquake expressed in terms of rock outcropping peak ground acceleration PGA_{rock} (in g) or peak ground velocity PGV_{rock} (in cm/s) or surface peak ground acceleration PGA_{surf} (in g), \widehat{IM} and β are the corresponding median values at which the structure reaches each damage limit state, LS, and log-standard deviation, respectively. A linear regression fit of the logarithms of the PGA_{rock} and u_x/H_{wall} , PGV_{rock} and u_x/H_{wall} as well as PGA_{surf} and u_x/H_{wall} data pairs which minimize the regression residuals is adopted. Indicatively, Figs. 13 and 14 illustrate plots (in logarithmic scale) of damage evolution in terms of u_x/H_{wall} (%) as a function of PGA_{rock} (in g) and PGV_{rock} (in m/s), respectively, for the two different quay wall configurations with W/H ratios equal to 0.6 and 0.8 as well as the corresponding limit u_x/H_{wall} values defined for each damage limit state.

Three components of uncertainty are accounted for related to the definition of the limit state value β_{LS} (defined empirically as $\beta_{LSi} = 0.4$), the capacity of each structural-type β_c (defined empirically as $\beta_c = 0.25$), and the demand β_D [47]. The demand β_D is calculated conducting statistical processing of the numerical results (IM and DM data pairs). In particular, we estimate the dispersion of the logarithms of PGA_{rock} and u_x/H_{wall} , as well as PGV_{rock} and u_x/H_{wall} data pairs obtained from the numerical analysis using the regression fit. The parameter β , which describes the total dispersion related to each fragility curve, is finally evaluated as the root of the sum of the squares of the three variability component dispersions assuming that they are statistically independent [47], as presented in the equation below:

$$\beta = \sqrt{\beta_{LS}^2 + \beta_c^2 + \beta_D^2} \tag{2}$$

We notice that compared to PGA_{rock} , following Luco and Cornell [39], PGV_{rock} seems to better correlate with structural deformation and damage (lower β_D values), providing useful and important information for an integrated fragility assessment.

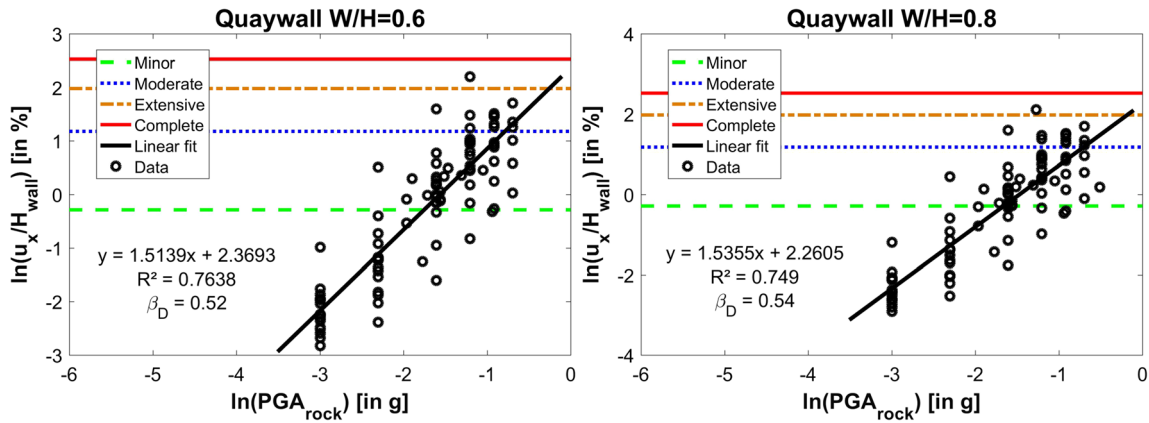


Fig. 13 PGA_{rock} (in g)– u_x/H_{wall} [%] relationship for the two different quay wall configurations with W/H ratios equal to 0.6 (left) and 0.8 (right)

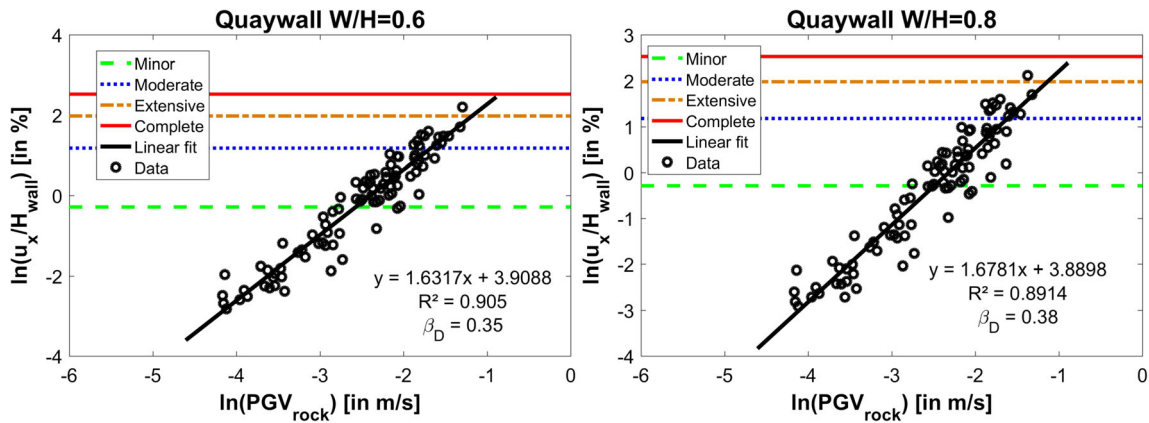


Fig. 14 PGV_{rock} (in m/s)– u_x/H_{wall} [%] relationship for the two different quay wall configurations with W/H ratios equal to 0.6 (left) and 0.8 (right)

Figures 15, 16 and 17 show the derived fragility curves along with their fragility parameters (median \overline{IM} and log-standard deviation β) in terms of PGA_{rock} , PGV_{rock} and PGA_{surf} , respectively, for the two different generic quay wall configurations with W/H ratios equal to 0.6 and 0.8 subjected to ground shaking for the two modelling approaches. It is noticed that fragility curves are developed for three damage states (e.g. corresponding to minor, moderate, extensive damage) while fragility curves for complete damage states are not provided. This is due to the fact that for both quay wall configurations, the corresponding limit values of u_x/H_{wall} (%) defined for complete damage state are not reached and thus fragility curves for complete damage are not proposed.

Once the probabilities of exceeding the predefined damage limit states are calculated, the vulnerability (or damage) index d_m for each level of seismic intensity can be estimated according to the following expression:

$$d_{mj} = \sum_{i=1}^4 P_{ij} \cdot d_i \tag{3}$$

where d_{mj} is the damage index (taking values from 0: no damage to 1: complete damage) corresponding to each seismic intensity level j , P_{ij} is the discrete damage probability for each damage limit state and d_i is the damage index at each damage limit state.

Following NIBS [47], we set the central value of the damage index at each damage limit state for the quay walls equal to 0.08, 0.275 and 0.70 for the LS1 (minor), LS2 (moderate) and LS3/LS4 (extensive/complete), respectively. A vulnerability curve is then generated which provides a unique damage index for each level of seismic intensity. Figure 18 shows the derived vulnerability curves in terms of PGA_{rock} , PGV_{rock} and PGA_{surf} and for the two different quay wall configurations with W/H ratios equal to 0.6 and 0.8 subjected to ground shaking considering soil

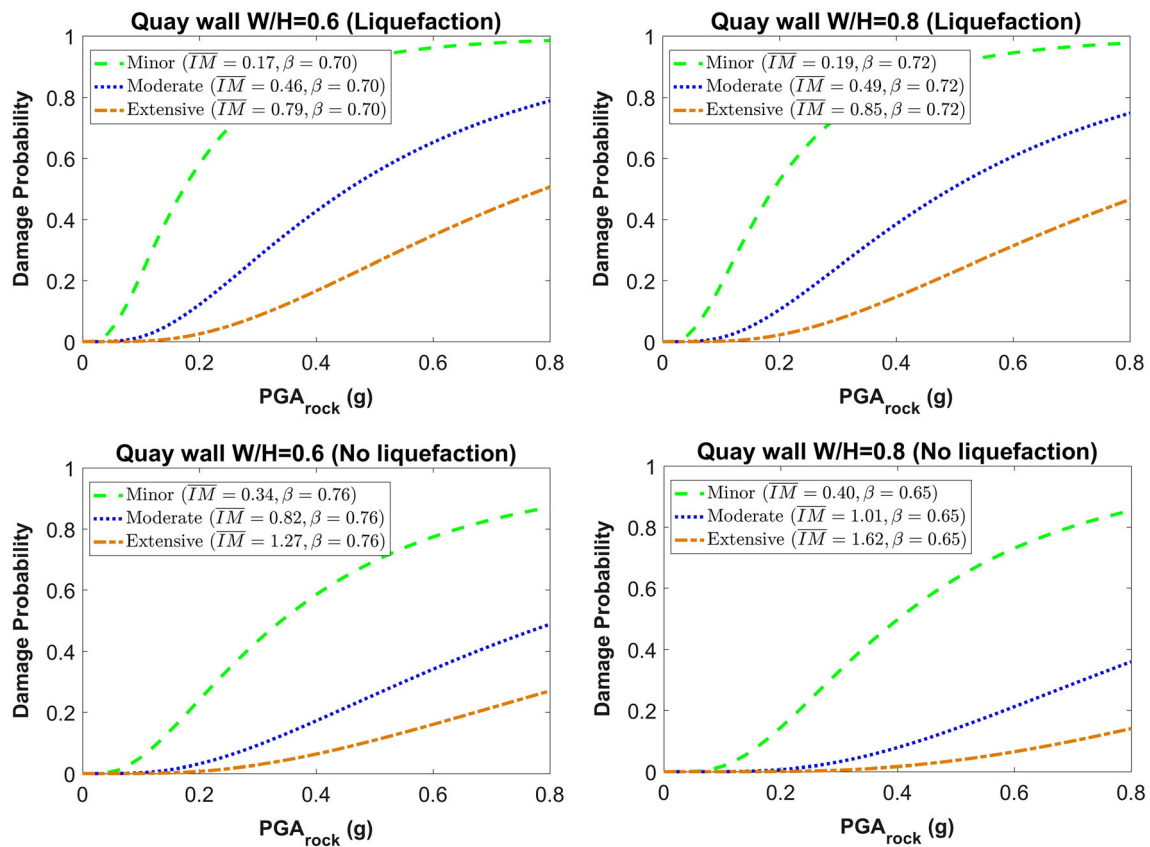


Fig. 15 Fragility curves in terms of PGA_{rock} for the two different quay wall configurations with W/H ratios equal to 0.6 (left) and 0.8 (right) considering (top) or not (bottom) liquefaction

liquefaction. With the vulnerability curves, structural losses of the quay walls are accounted for.

The most important observation through these figures is that when considering liquefaction the computed fragilities and the vulnerability are considerably increased independently of the IM used. The detrimental effect of soil liquefaction in terms of higher failure probabilities at all damage states is clearly obvious. This trend is noticeable for both examined quay wall configurations. The above findings are consistent with the observations of Calabrese and Lai [9]. A secondary remark is that the vulnerability of the quay wall is generally decreased when the W/H ratio increases. This is noticeable when considering all IMs, namely PGA_{rock} , PGV_{rock} and PGA_{surf} . This fact should be expected considering that the stiffer quay wall with the higher W/H ratio will sustain less horizontal displacement and therefore (for the same H_{wall}) less damage defined in terms of normalized residual seaward displacement (u_x/H_{wall}).

Finally, after comparing the fragility/vulnerability curves in terms of PGA_{rock} and PGV_{rock} we observe that

the curves in terms of PGV_{rock} are characterized by lower uncertainty, which is obvious from their lower slope compared to these in terms of PGA_{rock} . This fact is also proved by the lower standard deviation β value, which leads to a less flatter curve and thus to lower uncertainty.

5.3 Comparison with literature

In the following, we perform some comparisons between the herein resulted fragility curves with other relevant analytical ones from the literature to further enhance their validity. More specifically, in Fig. 19 we compare the proposed fragility curves for the quay wall with W/H ratio equal to 0.6 not considering liquefaction with the corresponding analytical ones derived in UPGRADE [57] where the same damage states are considered. We see that the comparison of the fragility curves for all damage states is rather good. A little lower failure probabilities for all damage states mainly at low ground intensities are proposed by UPGRADE [57], probably due to the fact that in that study the interfaces between the blocks of the quay

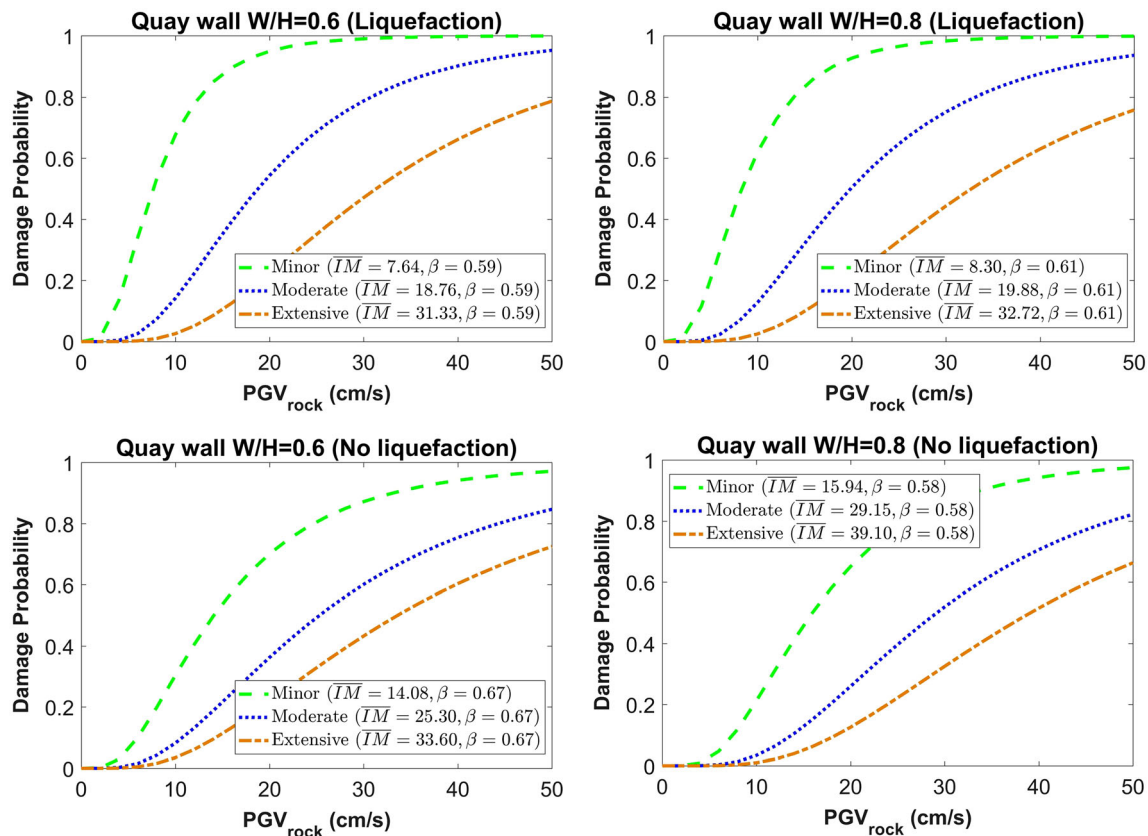


Fig. 16 Fragility curves in terms of PGV_{rock} for the two different quay wall configurations with W/H ratios equal to 0.6 (left) and 0.8 (right) considering (top) or not (bottom) liquefaction

wall configuration are considered and thus significant energy dissipation may occur during shaking.

Another comparison is conducted with the fragility curves derived by the study of Miraei and Jafarian [46] who conducted numerical analyses to study the seismic response of a quay wall which was previously modelled in centrifuge. They studied a quay wall configuration with W/H ratio equal to 0.5, while liquefaction occurred during the shaking produced horizontal displacement, settlement and tilting in the structure. For the derivation of fragility curves, they also considered the same damage states. They concluded that according to the fragility curves of system for lognormal distributions, the probability of failure for PGA_{rock} equal to 0.5 g in damage states I, II, and III is 98.5%, 53.1%, and 12.7%, respectively. In this study, we conclude that the probability of failure for the quay wall configuration with W/H ratio equal to 0.6 considering liquefaction and for PGA_{rock} equal to 0.5 g in damage states LS1, LS2, and LS3 is 93.4%, 55.3%, and 25.7%, respectively. Hence, considering the various uncertainties

involved, the comparison between the herein proposed fragility curves and the above literature fragility curves is generally satisfactory.

6 Summary and conclusions

In this study, we developed two modelling approaches to investigate the effect of liquefaction on the seismic performance and vulnerability of typical port gravity quay walls. The first is a soil–structure system subjected to seismic ground excitations avoiding liquefaction, while in the second the same soil–structure system is excited under effective stresses considering soil liquefaction. We examined different gravity quay wall configurations corresponding to different base width to height ratios. To get better insight on the seismic response of the coupled soil–wall system we conducted full dynamic analyses of a typical quay wall of Thessaloniki port where soil conditions are prone to liquefaction, as well as of two other

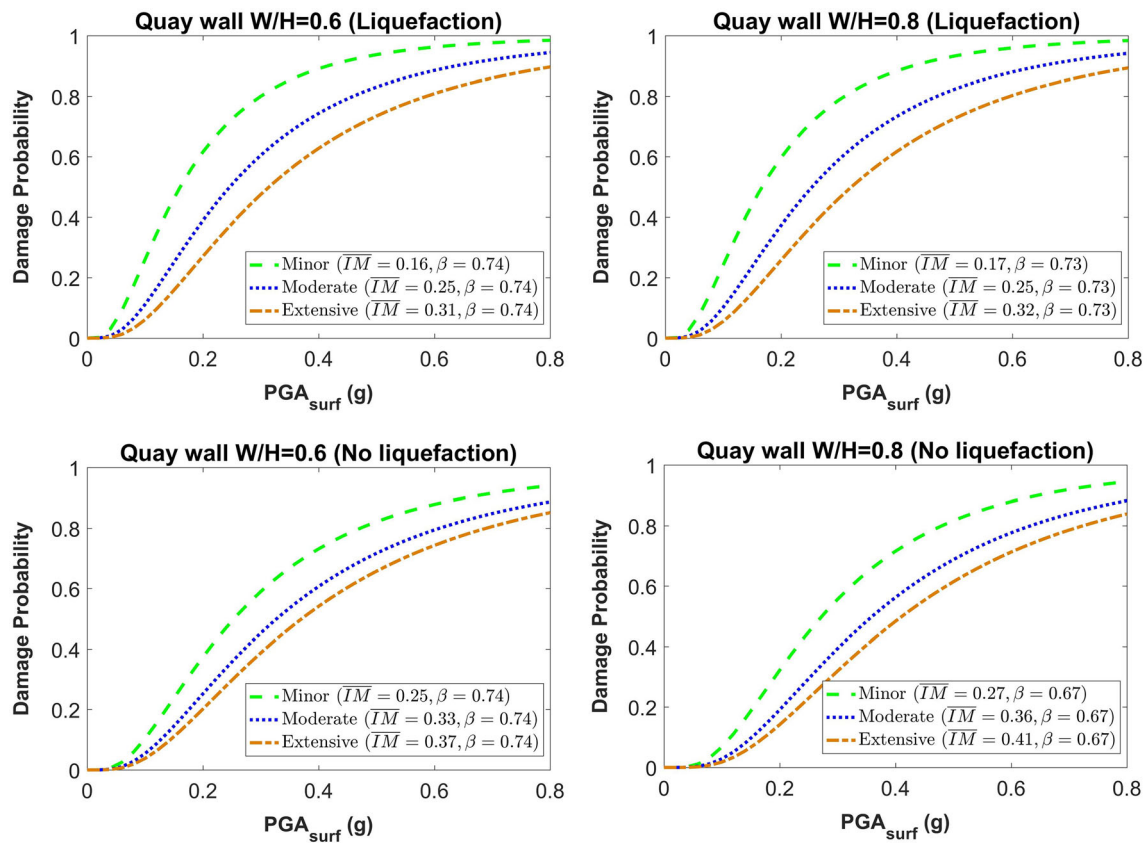


Fig. 17 Fragility curves in terms of PGA_{surf} for the two different quay wall configurations with W/H ratios equal to 0.6 (left) and 0.8 (right) considering (top) or not (bottom) liquefaction

generic quay wall configurations, for a number of strong ground excitations for the two modelling approaches, with and without liquefaction. Selected results were presented and discussed in terms of acceleration time histories at different locations on the wall and the soil, as well as in terms of the residual seaward displacement and the permanent vertical displacement of the quay wall. Then, we studied the effect of liquefaction and the geometry of a quay wall on its seismic vulnerability. We considered two generic configurations of the quay wall corresponding to base width-to-height (W/H) ratios of 0.6 and 0.8 and conducted incremental dynamic analysis. The damage measure was defined in terms of the normalized seaward displacements, which has been shown to result as an appropriate Damage Metric from the viewpoint of quay wall performance. Finally, we proposed fragility curves for different damage limit states and vulnerability curves as a function of PGA_{rock} , PGV_{rock} and PGA_{surf} .

The main conclusion of the comparative study is that while the impact of the liquefaction on the amplitude of the acceleration of the wall may be negligible compared to the non-liquefaction case, the effect on the permanent seaward horizontal and vertical displacements of the wall is found to be very important, increasing in that way considerably the vulnerability of the wall. Regarding the expected seismic damages of the quay wall, it has been shown that the vulnerability of the quay wall is generally decreased for the stiffer quay wall configuration (i.e. the one with the higher W/H ratio). The most important result of this study is the proof and in certain degree the quantification of the detrimental effect of liquefaction on the seismic vulnerability gravity quay walls. This fact is evident as an increase in the probability of failure for all damage states, and this holds for both quay wall configurations. Finally, the vulnerability in terms of PGV_{rock} is characterized by a lower level of uncertainty, as noted by the lower slope of the

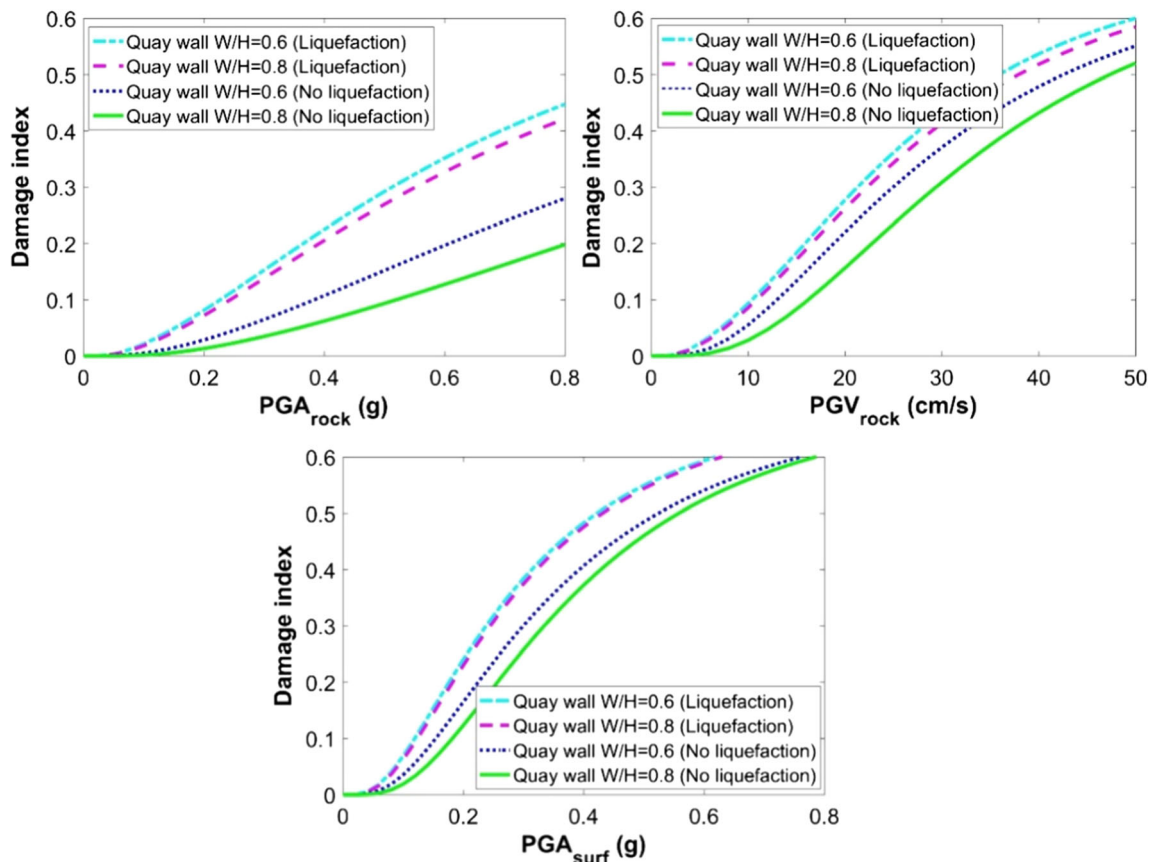


Fig. 18 Vulnerability curves in terms of PGA_{rock} (top-left), PGV_{rock} (top-right) and PGA_{surf} (bottom) for the two different quay wall configurations considering or not liquefaction

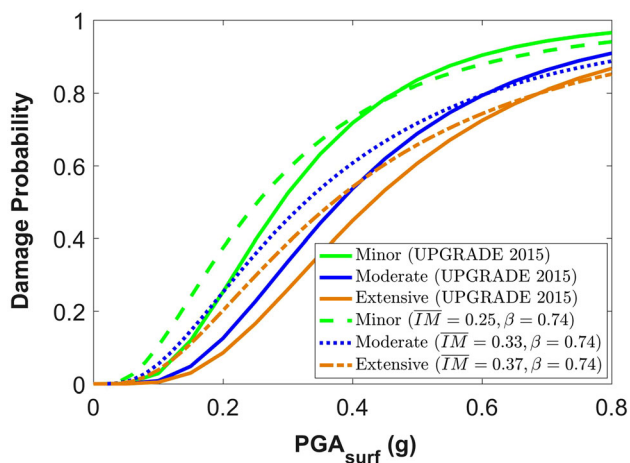


Fig. 19 Comparison of the proposed fragility curves for the quay wall with W/H ratio equal to 0.6 not considering liquefaction with the corresponding analytical ones of UPGRADE [57]

curves compared to that in terms of PGA_{rock} , an observation which leads to the remark that PGV_{rock} seems to have a better correlation with normalized residual seaward displacement demand and hence it might provide more

appropriate information for an integrated fragility assessment of gravity port quay walls.

Acknowledgements The authors would like to acknowledge the support by the project ‘‘Resilient, system-wide seismic risk assessment of port facilities. Application to Thessaloniki Port system’’ RESPORTS project (<http://resports.gr/>), funded by the Hellenic Foundation for Research and Innovation (HFRI) and General Secretariat for Research and Technology (GSRT) under Grant Agreement Number 754.

Authors’ contributions All authors contributed to the conceptualization of the study. The first draft of the manuscript was written by Dr. Stella Karafagka, who also conducted the analyses using the open-source computational software OpenSees, and all authors commented on previous versions of the manuscript. All authors read and approved the final manuscript.

Funding This study was funded by the Hellenic Foundation for Research and Innovation (HFRI) and General Secretariat for Research and Technology (GSRT) under Grant Agreement Number 754.

Availability of data and material Can be available after request following publication.

Code availability Can be available after request following publication.

Declarations

Conflict of interest The authors declare that they have no conflict of interest.

References

- Akkar S, Bommer JJ (2010) Empirical equations for the prediction of PGA, PGV and spectral accelerations in Europe, the Mediterranean and the Middle East. *Seismol Res Lett* 81:195–206
- Alielahi H, Moghadam MR (2017) Fragility curves evaluation for broken-back block quay walls. *J Earthq Eng* 21(1):1–22. <https://doi.org/10.1080/13632469.2016.1142487>
- Amipour S, Khashila M, Bayoumi A, Karray M, Chekired M (2022) Specimens size effect D/H on cyclic behaviour and liquefaction potential of clean sand. *Acta Geotech* 17:2047–2057. <https://doi.org/10.1007/s11440-021-01339-x>
- Anastasiadis A, Raptakis D, Pitilakis K (2001) Thessaloniki's detailed microzoning: subsurface structure as basis for site response analysis. *Pure Appl Geophys* 158(12):2597–2633
- Andrianopoulos KI, Papadimitriou AG, Bouckovalas GD (2010) Bounding surface plasticity model for the seismic liquefaction analysis of geostructures. *Soil Dyn Earthq Eng* 30:895–911
- Biot MA (1962) Mechanics of deformation and acoustic propagation in porous media. *J Appl* 33(4):1482–1498
- Bowen RM (1976) Theory of mixtures. In: Eringen AC (ed) *Continuum physics*, vol III. Academic Press, New York, pp 1–127
- Brinkgreve RBJ, Engin E, Swolfs WM (2017). *Plaxis 2D manual*. Rotterdam, Netherlands, Balkema
- Calabrese A, Lai CG (2013) Fragility functions of blockwork wharves using artificial neural networks. *Soil Dyn Earthq Eng* 52:88–102. <https://doi.org/10.1016/j.soildyn.2013.05.002>
- Calabrese A, Lai CG (2016) Sensitivity analysis of the seismic response of gravity quay walls to perturbations of input parameters. *Soil Dyn Earthq Eng* 82:55–62. <https://doi.org/10.1016/j.soildyn.2015.11.010>
- CEN EN 1998-1 (2004) Eurocode 8: Design of structures for earthquake resistance - Part 1: General rules, seismic actions and rules for buildings. European Committee for Standardization, Brussels
- CEN EN 1998-5 (2004) Eurocode 8: Design of structures for earthquake resistance - Part 5: Foundations, retaining structures and geotechnical aspects. European Committee for Standardization, Brussels
- Chang SE (2000) Disasters and transport systems: loss, recovery and competition at the Port of Kobe after the 1995 earthquake. *J Transp Geogr* 8(1):53–65. [https://doi.org/10.1016/S0966-6923\(99\)00023-X](https://doi.org/10.1016/S0966-6923(99)00023-X)
- Chiaradonna A, Özcebe AG, Bozzoni F, Fama A, Zuccolo E, Lai CG, Flora A, Cosentini RM, d'Onofrio A, Bilotta E, Silvestri F (2018) Numerical simulation of soil liquefaction during the 20 May 2012 M6.1 Emilia earthquake in Northern Italy: the case study of Pieve di Cento. In: Proceedings of the 16th European conference on earthquake engineering, pp 18–21 June, Thessaloniki, Greece
- Cubrinovski M, Green RA, Wotherspoon L (2011) *Geotechnical Reconnaissance of the 2011 Christchurch, New Zealand Earthquake*, vol 1, GEER Association Report 027
- Dafalias YF, Manzari MT (2004) Simple plasticity sand model accounting for fabric change effects. *J Eng Mech ASCE* 130(6):622–634
- Flora A, Bilotta E, Chiaradonna A, Lirer S, Mele L, Pingue L (2021) A field trial to test the efficiency of induced partial saturation and horizontal drains to mitigate the susceptibility of soils to liquefaction. *Bull Earthq Eng* 19:3835–3864. <https://doi.org/10.1007/s10518-020-00914-z>
- Gobbi S, Reiffsteck P, Lenti L, Santisi d'Avila MP, Semblat JF (2022) Liquefaction triggering in silty sands: effects of non-plastic fines and mixture-packing conditions. *Acta Geotech* 17:391–410. <https://doi.org/10.1007/s11440-021-01262-1>
- Goudarzy M, Sarkar D, Lieske W, Wichtmann T (2022) Influence of plastic fines content on the liquefaction susceptibility of sands: monotonic loading. *Acta Geotech* 17:1719–1737. <https://doi.org/10.1007/s11440-021-01283-w>
- Goudarzy M, Sarkar D, Wichtmann T (2022) Influence of plastic fines content on the liquefaction susceptibility of sands: cyclic loading. *Acta Geotech* 17:1719–1737. <https://doi.org/10.1007/s11440-022-01633-2>
- Ichii K (2003) Application of performance-based seismic design concept for caisson-type quay walls, PhD Dissertation, Kyoto University
- Ichii K (2004) Fragility curves for gravity-type quay walls based on effective stress analyses. In: Proceedings of the 13th world conference on earthquake engineering
- Iervolino I, Galasso C, Cosenza E (2010) REXEL: computer aided record selection for code-based seismic structural analysis. *Bull Earthq Eng* 8(2):339–362
- International Navigation Association – PIANC (2001) *Seismic design guidelines for port structures*. Chairman: Iai S, Bakelma Publishers, Tokyo
- Itasca (2019). *FLAC—fast Lagrangian analysis of continua, user's manual*, Version 8.1. Itasca Consulting Group, Inc., Minneapolis, Minnesota
- Jalayer F, Beck J, Zareian F (2012) Analyzing the sufficiency of alternative scalar and vector intensity measures of ground shaking based on information theory. *J Eng Mech* 138(3):307–316
- Jones KG, Morga M, Wanigarathna N, Pascale F, Meslem A (2021) Improving the resilience of existing built assets to earthquake induced liquefaction disaster events. *Bull Earthq Eng* 19:4145–4169. <https://doi.org/10.1007/s10518-020-00979-w>
- Joyner WB, Chen ATF (1975) Calculation of nonlinear ground response in earthquakes. *Bull Seismol Soc Am* 65(5):1315–1336
- Kakderi K, Pitilakis K (2010) Seismic performance and reliability of port facilities—the case of Thessaloniki (Greece). In: Proceedings of the 5th International conference on recent advances in geotechnical earthquake engineering and soil dynamics and symposium
- Kamalzadeh A, Pender MJ (2019) Modelling the dynamic response of gravity retaining wall systems using OpenSees. In: *Earthquake geotechnical engineering for protection and development of environment and constructions*, ISBN: 978-0-367-14328-2
- Karafagka S, Fotopoulou S, Pitilakis D (2021) Fragility curves of non-ductile RC frame buildings on saturated soils including liquefaction effects and soil-structure interaction. *Bull Earthq Eng* 19:6443–6468. <https://doi.org/10.1007/s10518-021-01081-5>
- Karafagka S, Fotopoulou S, Pitilakis D (2021) Fragility assessment of non-ductile RC frame buildings exposed to combined ground shaking and soil liquefaction considering SSI. *Eng Struct* 229:111629. <https://doi.org/10.1016/j.engstruct.2020.111629>
- Karakus H, Ergin BA, Guler I, Cihan K, Yuksel Y (2012) Dynamic response of block type quay wall. In: Proceedings of the 8th international conference on coastal and port engineering in developing countries, pp 20–24 Feb, IIT Madras, Chennai, India
- Karimi Z, Dashti S (2016) Seismic performance of shallow founded structures on liquefiable ground: validation of numerical

- simulations using centrifuge experiments. *J Geotech Geoenviron Eng ASCE* 142(6):04016011
35. Lai CG, Bozzoni F, Conca D et al (2021) Technical guidelines for the assessment of earthquake induced liquefaction hazard at urban scale. *Bull Earthq Eng* 19:4013–4057. <https://doi.org/10.1007/s10518-020-00951-8>
 36. Lee MG, Ha JG, Cho HI, Sun CG, Kim DS (2021) Improved performance-based seismic coefficient for gravity-type quay walls based on centrifuge test results. *Acta Geotech* 16:1187–1204. <https://doi.org/10.1007/s11440-020-01086-5>
 37. Ling HI, Yang S (2006) Unified sand model based on the critical state and generalized plasticity. *J Eng Mech ASCE* 132(12):1380–1391
 38. Lopez-Caballero F, Modaressi Farahmand-Razavi A (2008) Numerical simulation of liquefaction effects on seismic SSI. *Soil Dyn Earthq Eng* 28(2):85–98
 39. Luco N, Cornell CA (2007) Structure-specific scalar intensity measures for near-source and ordinary earthquake ground motions. *Earthq Spectra* 23(2):357–392
 40. Lysmer J, Kuhlemeyer AM (1969) Finite dynamic model for infinite media. *J Eng Mech Div ASCE* 95:859–877
 41. Malekmakan M, Shahir H, Ayoubi P (2021) Investigation of liquefaction-induced lateral spreading of gently sloping grounds using a variable permeability model. *Int J Numer Anal Methods Geomech* 45:1809–1832. <https://doi.org/10.1002/nag.3243>
 42. Manzari MT, Dafalias YF (1997) A two-surface critical plasticity model for sand. *Geotechnique* 47(2):255–272
 43. Masing G (1926) Eigenspannungen und verfertigung beim messing. In: *Proceedings of the 2nd international congress for applied mechanics, Zurich, Switzerland*
 44. Mazzoni S, McKenna F, Scott MH, Fenves GL (2009) Open system for earthquake engineering simulation user command-language manual, Pacific Earthquake Engineering Research Center, University of California, Berkeley
 45. Mele L (2022) An experimental study on the apparent viscosity of sandy soils: from liquefaction triggering to pseudo-plastic behaviour of liquefied sands. *Acta Geotech* 17:463–481. <https://doi.org/10.1007/s11440-021-01261-2>
 46. Miraei M, Jafarian Y (2013) Fragility curves for assessing the seismic vulnerability of gravity quay walls. In: *Proceedings of the 4th COMPDYN, Kos Island, Greece*
 47. National Institute of Building Sciences -NIBS (2004) Multi-hazard Loss Estimation Methodology Earthquake Model. HAZUS-MH Technical manual, Federal Emergency Management Agency, Washington, D.C.
 48. Papadimitriou AG, Bouckovalas GD (2002) Plasticity model for sand under small and large cyclic strains: a multiaxial formulation. *Soil Dyn Earthq Eng* 22(3):191–204. [https://doi.org/10.1016/S0267-7261\(02\)00009-X](https://doi.org/10.1016/S0267-7261(02)00009-X)
 49. Parra E (1996) Numerical modelling of liquefaction and lateral ground deformation including cyclic mobility and dilation response in soil systems, Ph.D. thesis, Rensselaer Polytechnic Institute, Troy, NY
 50. Pastor M, Zienkiewicz OC, Chan AHC (1990) Generalized plasticity and the modeling of soil behaviour. *Int J Numer Anal Methods Geomech* 14(3):151–190
 51. Pitilakis K, Argyroudis S, Fotopoulou S, Karafagka S, Kakderi K, Selva J (2019) Application of stress test concepts for port infrastructures against natural hazards. The case of Thessaloniki port in Greece. *Reliab Eng Syst Saf* 184:240–257
 52. Pitilakis K, Moutsakis A (1989) Seismic analysis and behaviour of gravity retaining walls. The case of Kalamata harbour quay-wall. *Soils Found* 29(1):1–17. <https://doi.org/10.3208/sandf1972.29.1>
 53. Prevost JH (1985) A simple plasticity theory for frictional cohesionless soils. *Soil Dyn Earthq Eng* 4:9–17
 54. Ramirez J, Barrero AR, Chen L, Dashti S, Ghofrani A, Taiebat M, Arduino P (2018) Site response in a layered liquefiable deposit: evaluation of different numerical tools and methodologies with centrifuge experimental results. *J Geotech Geoenviron Eng* 144(10):04018073
 55. Stewart JP, Kwok AO, Hashash YMA, Matasovic N, Pyke R, Wang Z, Yang Z (2008). Benchmarking of nonlinear geotechnical ground response analysis procedures, PEER Report No. 2008/04, Pacific Earthquake Engineering Research Center, University of California, Berkeley, CA
 56. Sun Z, Chu J, Xiao Y (2021) Formulation and implementation of an elastoplastic constitutive model for sand-fines mixtures. *Int J Numer Anal Methods Geomech* 45:2682–2708. <https://doi.org/10.1002/nag.3282>
 57. UPGRADE Research project (2015) Deliverable D8.2 Technical reports with the calculation results of the vulnerability of specific Greek port facilities (in Greek)
 58. Vamvatsikos D, Cornell CA (2002) Incremental dynamic analysis. *Earthq Eng Struct Dyn* 31(3):491–514
 59. Vamvatsikos D, Cornell CA (2005) Developing efficient scalar and vector intensity measures for IDA capacity estimation by incorporating elastic spectral shape information. *Earthq Eng Struct Dyn* 34(13):1573–1600
 60. Yang Z (2000) Numerical modelling of earthquake site response including dilation and liquefaction, Ph.D. thesis, Columbia University, New York
 61. Yang Z, Elgamal A (2003) Application of unconstrained optimization and sensitivity analysis to calibration of a soil constitutive model. *Int J Numer Anal Methods Geomech* 27(15):1277–1297
 62. Yang Z, Elgamal A, Parra E (2003) Computational model for cyclic mobility and associated shear deformation. *J Geotech Geoenviron Eng* 129(12):1119–1127
 63. Yang J, Liang LB, Chen Y (2022) Instability and liquefaction flow slide of granular soils: the role of initial shear stress. *Acta Geotech* 17:65–79. <https://doi.org/10.1007/s11440-021-01200-1>
 64. Yang Z, Lu J, Elgamal A (2008) OpenSees soil models and solid-fluid fully coupled elements. User's manual, version 1.0. Department of Structural Engineering, University of California, San Diego

Publisher's Note Springer Nature remains neutral with regard to jurisdictional claims in published maps and institutional affiliations.

Springer Nature or its licensor (e.g. a society or other partner) holds exclusive rights to this article under a publishing agreement with the author(s) or other rightsholder(s); author self-archiving of the accepted manuscript version of this article is solely governed by the terms of such publishing agreement and applicable law.